Sounding of the Atmosphere using Broadband Emission Radiometry (SABER):

Instrument and Science Measurement Description

The SABER Team:

Roy Esplin (Space Dynamics Laboratory, Logan, UT)

Martin Mlynczak (NASA Langley Research Center, Hampton, VA)

James Russell (Hampton University, Hampton, VA)

Larry Gordley (GATS Inc., Newport News, VA)

Doran Baker (Utah State University, Logan, UT (deceased))

Kenneth Beaumont (NASA Langley Research Center, Hampton, VA)

Guy Beaver (GATS, Inc., Newport News, VA (formerly))

Christopher Brown (NASA Langley Research Center, Hampton, VA)

Steven Brown (Space Dynamics Laboratory, Logan, UT)

Michael Cisewski (NASA Langley Research Center, Hampton, VA)

Todd Denkins (NASA Langley Research Center, Hampton, VA)

John Dodgen (NASA Langley Research Center, Hampton, VA (deceased))

James Dyer (Space Dynamics Laboratory, Logan, UT (retired))

Thomas Eden (LASP, University of Colorado, Boulder, CO)

Patrick Espy (Norwegian University of Science and Technology, Trondheim, Norway)

Matt Felt (Space Dynamics Laboratory, Logan, UT)

Rolando Garcia (National Center for Atmospheric Research, Boulder, CO)

Richard Grube (NASA Langley Research Center, Hampton, VA)

Glen Hansen (Space Dynamics Laboratory, Logan, UT)

Scott Hansen (Space Dynamics Laboratory, Logan, UT)

Susan Henriksen (NASA Langley Research Center, Hampton, VA (retired))

Linda Hunt (Science Systems and Applications, Inc., Hampton, VA)

William Grose (NASA Langley Research Center, Hampton, VA (retired))

Ron Huppi (Space Dynamics Laboratory, Logan, UT (retired))

28 Antony Jalink (NASA Langley Research Center, Hampton, VA (deceased))

29 Mark Jensen (Space Dynamics Laboratory, Logan, UT)

30 Scott Jensen (Orion Space Solutions, Louisville, CO)

31 Gretchen Lingenfelser (NASA Langley Research Center, Hampton, VA (retired))

32 Manuel Lopez Puertas (Instituto de Astrofisica de Andalucia, Granada, Spain)

33 Benjamin Marshall (GATS, Inc., Newport News, VA)

34 Mark Melbert (GATS, Inc., Newport News, VA (formerly))

35 Christopher Mertens (NASA Langley Research Center, Hampton, VA)

36 James Miller (NASA Langley Research Center, Hampton, VA (deceased))

37 Keith Paskett (Space Dynamics Laboratory, Logan, UT)

38 Gregory Paxton (GATS, Inc., Newport News, VA)

39 Frank Peri (NASA Langley Research Center, Hampton, VA)

40 James Petersen (Space Dynamics Laboratory, Logan, UT)

41 Richard Picard (Air Force Resarch Laboratory, Hanscom AFB, (retired))

42 Ellis Remsberg (NASA Langley Research Center, Hampton, VA)

43 Donald Robinson (NASA Langley Research Center, Hampton, VA (deceased))

44 Raymond Roble (National Center for Atmospheric Research, retired)

45 William Roettker (Ball Aerospace, Boulder, CO)

46 Deron Scott (Space Dynamics Laboratory, Logan, UT)

47 Robert Sherrill (NASA Langley Research Center, Hampton, VA (retired))

48 Andrew Shumway (Space Dynamics Laboratory, Logan, UT)

49 David Siskind (Naval Research Laboratory, Washington, DC, retired)

50 Susan Solomon (Massachusetts Institute of Technology, Boston, MA)

51 John Stauder (Space Dynamics Laboratory, Logan, UT)

52 Kenneth Stone (University of Colorado, Boulder, CO)

53 Charles Stump (NASA Langley Research Center, Hampton, VA (retired))

54 Joe Tansock (Utah State University, Logan, UT)

55 R. Thompson (GATS, Inc., Newport News, VA (retired))

56   Michael Vanek (NASA Langley Research Center, Hampton, VA (retired))

57   Yunfei Wang (GATS, Inc, Newport News, VA (formerly))

58   Jeremy Winick (Air Force Research Laboratory, Hanscom AFB, (retired))

59   Peter Wintersteiner (ARCON Corp., Waltham, MA (retired))

60   James Wells (NASA Langley Research Center, Hampton, VA)

61   John Wells (NASA Langley Research Center, Hampton, VA (retired))

62   James Ulwick (Stewart Radiance Laboratory, Bedford, MA (deceased))

63   Lorin Zollinger (Space Dynamics Laboratory, Logan, UT)

64   **Abstract**

65   SABER (Sounding of the Atmosphere using Broadband Emission Radiometry) is a 10-

66   channel infrared radiometer that is one of four instruments on the NASA TIMED (Thermosphere-

67   Ionosphere-Mesosphere Energetics and Dynamics) satellite mission to study the structure,

68   energetics, chemistry, and dynamics of the Earth's mesosphere and lower thermosphere. The

69   TIMED spacecraft was launched into a 625 km circular polar orbit (74.1° inclination) via a Boeing

70   Delta II rocket from Vandenberg Air Force Base on 7 December 2001. SABER continues to

71   operate nominally and collect data routinely as it has for over 21 years. Over 2,200 peer-reviewed

72   journal articles have been published worldwide using SABER data. A list of these articles is

73   included in the Supporting Information accompanying this paper. The Space Dynamics Laboratory

74   (SDL) of Utah State University designed, fabricated, and calibrated the SABER instrument in close

75   collaboration with NASA Langley Research Center, Hampton University, and Global

76   Atmospheric Technologies and Science (GATS). This paper provides a detailed technical

77   description of the SABER instrument, including performance specifications and observed

78   instrument performance.

Plain Language Summary

Earth's mesosphere and lower thermosphere (MLT), approximately 50 to 180 km in altitude or 30 to 110 miles high) was the least explored region of the atmosphere thirty years ago. The MLT is a critical region of Earth's atmosphere as it is the boundary or interface between the space environment and the lower atmosphere. Today the region is referred to as part of the 'geospace' environment. To examine the MLT in more detail, NASA developed the Thermosphere-Ionosphere-Mesosphere Energetics and Dynamics or TIMED satellite mission beginning in 1996. Launch of the TIMED satellite occurred in December 2001. One of the four instruments carried by the TIMED satellite is named SABER (Sounding of the Atmosphere using Broadband Emission Radiometry). SABER continues to provide exceptional scientific results and is still routinely collecting data more than 21 years after launch. This paper provides a technical description of the SABER instrument.

Key Points

1. SABER is an infrared limb sounding instrument observing the Earth's mesosphere and lower thermosphere continuously for over two decades.

2. SABER was developed through a partnership involving NASA Langley, Space Dynamics Laboratory, Hampton University, and GATS.

3. SABER is still operational with no reduction in capability and has yielded over 2,200 peer-reviewed journal articles by worldwide authors.

1. Introduction

This paper provides a detailed technical description of the Sounding of the Atmosphere using Broadband Emission Radiometry (SABER) instrument. SABER is one of four instruments on the Thermosphere-Ionosphere-Mesosphere Energetics and Dynamics (TIMED) satellite mission developed through the Heliophysics Division of NASA's Science Mission Directorate. The TIMED mission was developed to conduct the first comprehensive and global examination of the Earth's mesosphere and lower thermosphere (MLT), nominally the region between 60 and 180 km altitude. SABER was proposed in 1992 to the NASA Announcement of Opportunity (AO) for the TIMED mission. The TIMED AO was issued following mission Science Definition Team activities from 1990 to 1991. The TIMED mission entered formulation (Phase C) in October 1996 and four instruments were built and shipped for integration onto the TIMED spacecraft by the end of 1999. The SABER instrument was developed under a partnership between the NASA Langley Research Center, the Space Dynamics Laboratory (SDL) of Utah State University, Hampton University, and Global Atmospheric Technologies and Sciences (GATS). The TIMED spacecraft was launched into a 625 km circular orbit (74.1° inclination) via a Boeing Delta II rocket from Vandenberg Air Force Base on 7 December 2001. Routine SABER operations began 22 January 2002 and continue to this day with over 98% of all possible data collected. The TIMED mission is currently approved to continue routine operations through September 2023 and the mission team has proposed to NASA to continue another three years through September 2026. TIMED and SABER are among NASA's longest serving Earth-observing satellites and instruments. Continued observations of the geospace environment are critical as this region is now undergoing long-term change due to increasing carbon dioxide (*Mlynczak et al.*, 2021, 2023).

The SABER experiment was developed to conduct a comprehensive investigation into the thermal structure and energy balance of the MLT. The major elements of the energy budget are heating due to the absorption of solar radiation; heating due to exothermic chemical reactions that ultimately degrade much of the solar energy to heat; and infrared radiative cooling. *Mlynczak and Solomon* (1993) discuss in detail the entire chain of solar energy deposition, airglow (non-cooling) radiative losses, and heating through exothermic chemical reactions. Observations of kinetic temperature (T), ozone (O_3), water vapor (H_2O), carbon dioxide (CO_2), nitric oxide (NO), atomic oxygen (O), and atomic hydrogen (H) are required to fully characterize the radiative energy budget of the MLT (*Mlynczak*, 1996; 1997). From these measurements the vertical profiles of the rates of radiative heating and cooling and rates of heating due to exothermic chemical reactions may be derived. Every day, SABER provides approximately 1,400 profiles each of temperature, minor constituents (O_3, H_2O, CO_2, O, H), and more than 30 individual rates of radiative heating, radiative cooling, and rates of heating due to exothermic chemical reactions.

The scientific productivity of SABER has been exceptional. Over 2,200 peer-reviewed journal articles incorporating SABER data have been published worldwide. A list of reference citations to these articles is included in the Supporting Information to this paper. In addition, SABER data have been used in over 80 doctoral dissertations and master's theses, and in more than 120 books or book chapters. Over 1,000 presentations using SABER data have been made at scientific symposia.

SABER's success is due to the excellent quality of the infrared limb radiances that it measures. As mentioned earlier, approximately 1,400 profiles of infrared limb radiance (units of $W\ m^{-2}\ sr^{-1}$), per each of the 10 channels, are measured daily, resulting in over 100 million individual limb radiance profiles measured to date by SABER. Figure 1 illustrates the remarkable

radiometric performance of the SABER instrument. Shown in this figure are orbit-average limb

radiance profiles as a function of tangent altitude in each of the 10 SABER channels (described

below in more detail). The red profiles are data taken approximately two years after launch in 2003

during conditions near the maximum of the 11-year solar cycle. The blue profiles are taken 16.5

years later during solar minimum conditions. The vertical dashed line in each figure marks the

noise equivalent radiance (NER) value in each channel. The NER measured during ground

calibration of SABER are listed later in Section 3.1 in Table 2. The altitude at which the NER line

intersects the radiance profile is where the signal-to-noise is equal to unity. SABER routinely

observes limb radiance to a minimum upper limit of 100 km and to above 270 km in the nitric

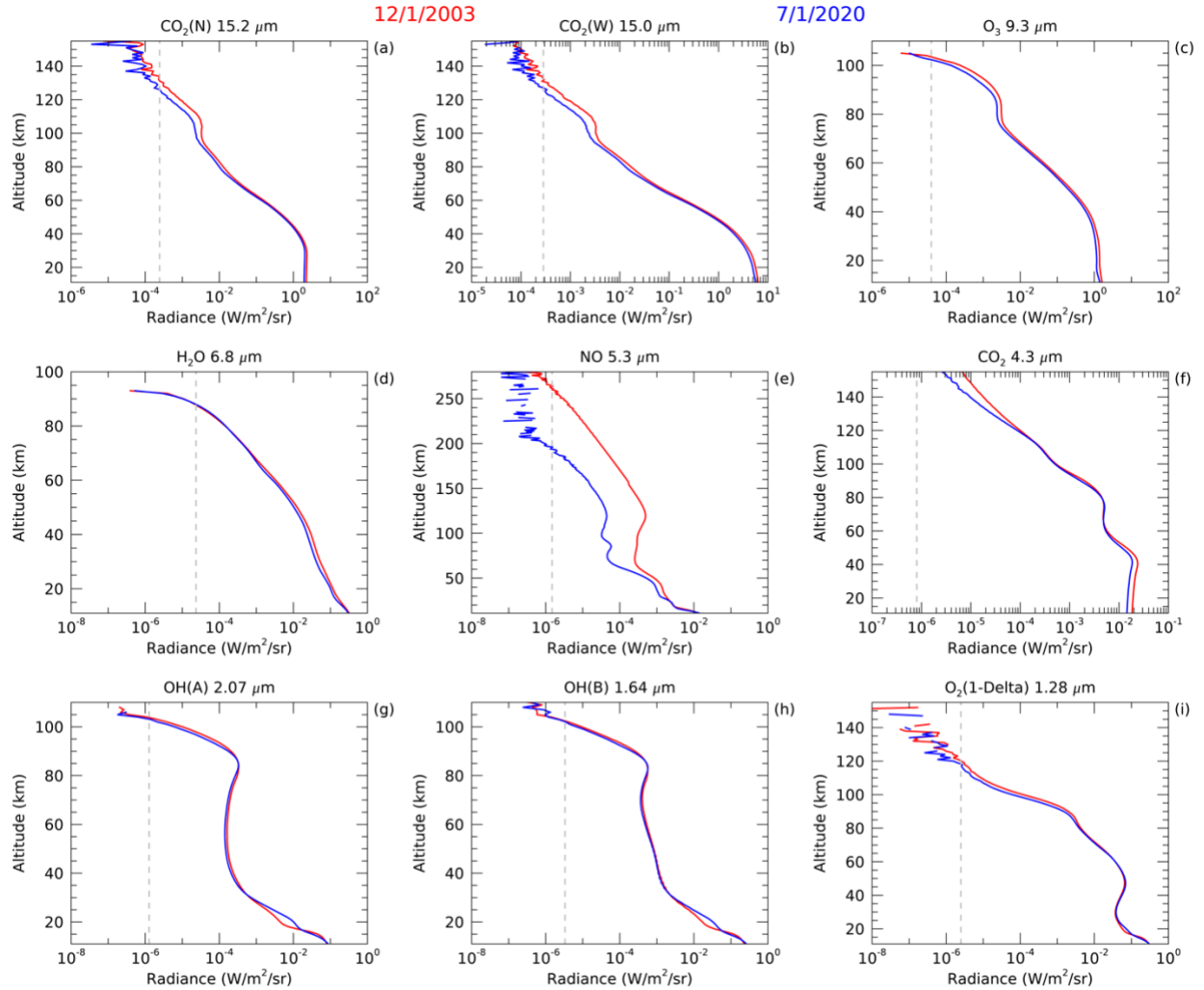oxide (NO) channel during solar maximum conditions.

Figure 1. Orbit average infrared limb radiance profiles (blue, red curves) and the corresponding noise equivalent radiance (NER, dashed vertical line) in each of SABER's 10 channels. The blue profiles were measured by SABER on 1 December 2003 and the red profiles on 1 January 2020.

This paper presents a detailed technical description of the SABER instrument including description of major subsystems of the instrument and technical performance parameters. The motivation for this paper is to describe the SABER instrument components and performance to document this information for future reference and satisfy NASA requirements in this regard.

8

164   The SABER instrument and preliminary calibration performance is described in *Russell,*

165   *Mlynczak*, et al., [1999]. The single most important decision made in the development of SABER

166   was to commit to producing the most accurately calibrated instrument possible for the available

167   resources. This one decision guided parts development, parts testing and selection, instrument

168   thermal and mechanical design, and instrument operations. The decision to focus on calibration

169   resulted in an instrument that is remarkably stable (as discussed in detail in *Mlynczak, Daniels*, et

170   al., 2020) and that has lasted well beyond the two-year lifetime envisioned for the TIMED mission.

171   The design and initial performance of SABER is described by *Brown et al*. (2006). The calibration

172   of SABER is described by *Tansock et al*. [2003]. The present paper describes the instrument and

173   components in much greater detail and provides final instrument design and performance

174   parameters. The complete SABER instrument calibration final report prepared by SDL for NASA

175   Langley is included in the Supporting Information.

176   The remainder of this paper is organized as follows: Section 2 describes the SABER

177   instrument and its operation; Section 3 describes many instrument level parameters including

178   radiometric, optical, and electrical in addition to parameters such as mass and size; Section 4

179   describes twelve major components of the SABER instrument (e.g., the in-flight calibrator and the

180   cryocooler); and the paper concludes with a Summary. Lastly, we note that the success of the

181   SABER instrument is due to the remarkable efforts of many people at the partner organizations.

182   Consequently, this paper contains a large team authorship.

183   **2. The SABER Instrument**

184   Figure 2 shows a computer-generated drawing of the of the SABER instrument and traces

185   the path of light from the scan mirror (C) to the focal plane array (O). Each letter in the figure

186   corresponds to a specific component or part of the instrument, which are listed in the legend to the

right of Figure 2. The SABER instrument is 103 cm in height, 60 cm from front to back, and 75 cm side to side. Light enters the instrument from the Earth's limb through the entrance aperture at point X. Thin green lines in the figure trace the path of the light through the fore-optics baffle (B) onto the scan mirror (C) which directs the light into a telescope with a series of mirrors (M1 through M4, items H, J, L, M in Figure 2). The scan mirror (C, D) can rotate to view the inflight calibrator (E, F) that is viewed every four limb scans. The inflight calibrator is a blackbody maintained at a temperature of 247 Kelvin. The mirror scans high enough to see a space view at approximately 400 km above the Earth's surface. The space view and the inflight calibrator provide the two-point reference needed to keep SABER calibrated over the life of the mission.
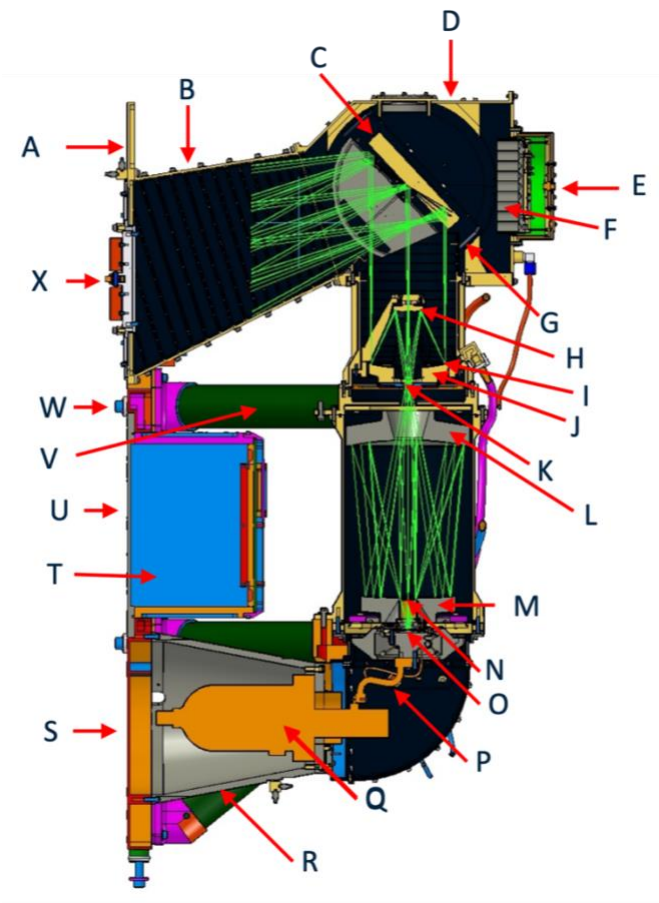
Letter Identifier	Component
A	Telescope Radiator
B	Fore-Optics Baffle
C	Scan Mirror
D	Scan Mirror Assembly
E	Inflight Calibrator (IFC) Assembly
F	Full-Aperture Blackbody & Jones Sources
G	In-Flight Calibrator Light Trap
H	Secondary Mirror (M2) with Sec. Mirror Baffle
I	Aperture Stop
J	Primary Mirror (M1) with Inner Conical Baffle
K	10 Aperture Chopper
L	Quaternary Mirror (M4)
M	Tertiary Mirror (M3)
N	Lyot Stop
O	Focal Plane Assembly (FPA)
P	Flexible Thermal Strap
Q	Cryocooler
R	Cryocooler Mount
S	Spacecraft Interface plate & cryocooler radiator
T	Electronics Box
U	Electronics Radiator
V	Telescope Support Strut (G-10 Fiberglass)
W	Alignment Cube (Removed before flight)
X	Cover (Ejected after initial outgassing)

Figure 2. Computer-generated internal view of the SABER instrument.

199   After passing through the series of mirrors the light is focused on the focal plane assembly

200   (O) that contains 10 discrete detectors. An interference filter over each detector provides spectral

201   isolation needed to quantify the infrared emission from CO_2, O_3, H_2O, OH, NO, and $O_2(^1\Delta)$. The

202   spectral bandpass for each channel can be seen later in Section 3.1 in Table 1. The focal plane is

203   cooled to 75 K by the miniature cryocooler (Q). A thermal strap (P) couples the cold finger of the

204   cryocooler to the detector focal plane. Cryogenic cooling is required to reduce thermal noise in the

205   detectors. The light entering the SABER telescope is also chopped (K) to create an AC signal that

206   can be synchronously detected and thereby readily distinguished from the large infrared DC

207   background of the instrument. More detail on the instrument design and operation is given below.

208   The Johns Hopkins University Applied Physics Laboratory (APL) designed and fabricated

209   the TIMED spacecraft. Figure 3 shows the SABER instrument installed in the TIMED spacecraft

210   at APL. The extent of the front surface of SABER can be identified by the planar white surfaces,

211   which are SABER's radiators. The darker oval surface in the smaller, white-surfaced radiator is

212   the covered entrance aperture to the instrument.

213

Figure 3. The SABER instrument installed in the TIMED spacecraft.

215

2.1 Detailed Instrument Description

A photograph of the assembled SABER instrument before it was covered by multilayer insulation (MLI) is shown in Figure 4. The instrument view is rotated 90 degrees to the left from the view in Figure 2. MLI blanketing details are described later in Section 2.1.1, SABER Purge and Vent System. The long G-10 fiberglass legs (the tan colored struts in Figure 4) thermally isolate the optics (contained in the cylindrical-shaped tube) from the SABER/spacecraft interface plate. Thermal, envelope, mass, and moment of inertia parameter values are summarized in Table 6 in Section 3.4. Component parameter values and descriptions are given in the component section of this paper (Section 4).
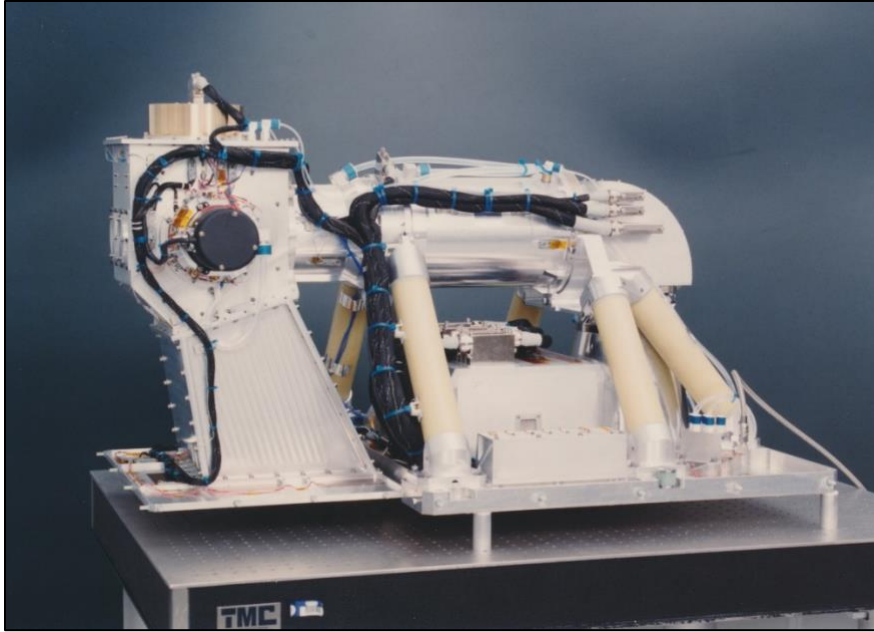
225

Figure 4. Assembled SABER instrument before it was covered with multi-layer insulation.

227

228   A functional block diagram of the SABER instrument is shown in Figure 5. This block

229   diagram (also see Figure 2) shows that incoming radiance from the Earth limb is focused on to a

230   mechanical chopper (operating at a frequency of 1000 Hz) by mirrors M1 and M2, which form a

231   Ritchey-Chrétien telescope, and are then reimaged by a clamshell re-imager consisting of mirrors

232   M3 and M4 onto a focal plane assembly (FPA). This FPA contains a Lyot stop, an array of 10

233   detectors covered by an array of 10 passband filters, 10 matched junction-gate field effect transistor

234   (JFET) pairs, and 10 feedback resistors. The JFET pairs and feedback resistors form the input

235   stages of 10 transimpedance amplifiers (TIA). The TIA input stages are connected by low thermal

236   conductance stainless steel wires to the remaining TIA components which are located inside the

237   electronics box.

13

Cover Release Actuator

Baffle   Light Trap

IFC Blackbody

Instrument Electronics

Cover Control

Throw Away Cover

IFC Jones Sources

Scan Mirror Drive/Control

IFC Sources Control

Scan Mirror

Data

Limb Radiance

Light Trap

1553 Interface   Commands

M2

Telescope Temperature 215 to 250 K

System Control & Data Handling

Telescope Radiator, temperature 208 to 235 K (Zone 1)

Chopper

M1

Chopper Electronics

M4

Operational Heaters Motor/Encoder Refrigerator

Operational Heater Power

Spacecraft Interface Plate, temperature 250 to 300 K (Zone 2)

Multiplexer & A/D

Chopper Sync

Phase-Lock Amps

Lyot Stop @ 75 K (Zone 3)

M3

Preamps

Power Distribution   Instrument Power

Electronics/ Refrigerator Radiator, temperature 240 to 265 K (Zone 2)

10 Channel FPA Module @75 K (Zone 3)

Filters

Detectors, matched JFET pairs, & Feedback Resistors

1553 Commands & Data

Refrigerator Mount   Refrigerator

Refrigerator Electronics (RFE)

Survival Heaters

Survival Heater Power

Refrigerator Cold Block @ 72 K

Motor/Encoder Refrigerator

250 to 270 K

Thermal tie to Interface Plate

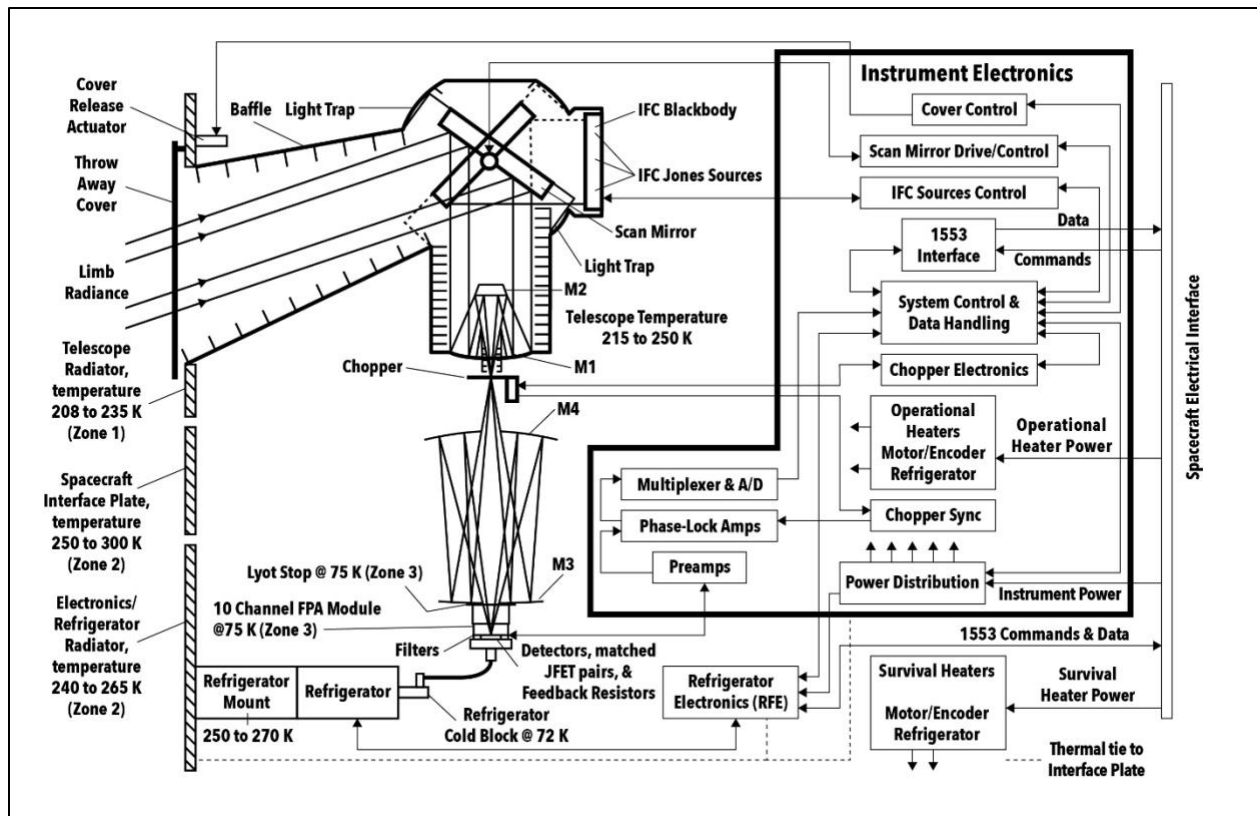Spacecraft Electrical Interface

Figure 5. SABER functional block diagram.

The chopped signals measured by the 10 detectors are amplified by the 10 TIA preamplifiers and then demodulated by 10 phase lock amplifiers and multiplexed into a single analog to digital (A/D) converter that converts the analog signals to digital signals. These digital signals are transferred to the spacecraft by means of a 1553 interface. A one-axis scan mirror with the axis of rotation on the mirror surface to prevent optical beam walk, scans the field of view (FOV) from hard Earth to cold space (approximately 400 km tangent altitude) and periodically points the FOV at an in-flight calibrator (IFC), which consists of a full-aperture blackbody and three partial aperture Jones sources.

The SABER instrument has three separate temperature zones as shown in Figure 5: Zone 1 which includes the telescope zone at temperature of 208 K to 250 K; Zone 2 which includes the

electronics/refrigerator zone at a temperature of 240 K to 270 K; and Zone 3, the FPA zone at a temperature of 75 K. Zone 1 consists of the telescope radiator, the telescope, the scan mirror, the IFC, the optical baffles, and the chopper mechanism. The telescope radiator is used when looking at deep space past the Earth limb and cools the telescope to reduce photon noise, reduces the heat load on the refrigerator, and minimizes the temperature of the full-aperture blackbody. The spacecraft undergoes a yaw maneuver every 60 days so that the telescope radiator and aperture, which are parallel to the orbit plane, are never exposed to direct sunlight. The telescope is thermally isolated from the warmer SABER support structure and the TIMED spacecraft bus by thermal blankets and telescope support struts (as shown in Figure 4).

Zone 2 consists of the electronics/refrigerator radiator, all electronics except the electronics inside the FPA, the refrigerator, and the TIMED spacecraft interface plate. The electronics box is bolted directly to the backside of the electronics/refrigerator radiator. Because the reject temperature of the refrigerator plays an important role in the overall cooling capacity of the refrigerator, precise control of the refrigerator reject temperature was needed. The SABER control electronics can operate under a wide range of temperatures without significantly affecting their performance.

Zone 3 consists of the FPA housing, a Lyot stop, 10 optical bandpass filters, 10 detectors, 10 matched JFET pairs, and 10 feedback resistors. The FPA is cooled through a flexible heat strap connected to a cryogenic pulse-tube refrigerator. The operation of the SABER instrument is described later in this section, and additional descriptions of its components are given in the component section of this paper.

The SABER telescope consists of an ejectable aperture cover with a wax-actuator cover release mechanism, a baffle, an optics radiator, a spacecraft interface plate that also serves as the

15

274 electronics and cryogenic cooler radiator, a single-axis scan mirror, a light trap around the scan

275 mirror, a Ritchey-Chrétien telescope consisting of mirrors M1 and M2, a chopper, a two-mirror

276 clamshell re-imager consisting of mirrors M3 and M4, an FPA, a power distribution and

277 conditioning box, a cover controller, a scan mirror driver, an IFC, and an IFC temperature

278 controller, chopper electronics, operational heaters, survival heaters, and a scan mirror angle

279 encoder.

280   The scan mirror continually scans the SABER FOV from hard Earth to deep space and

281 back. Periodically, the scan mirror also points the FOV at the IFC. M1 and M2 focus the Earth

282 limb radiance onto a 10-aperture chopper which amplitude modulates the radiance. M3 and M4

283 reimage the modulated light onto 10 discrete detectors in the FPA. The FPA consists of a Lyot

284 stop, an array of 10 filters, an array of 10 detectors, and an array of JFET pairs and feedback

285 resistor-capacitor combinations that determine the spectral parameters of the SABER instrument.

286   The SABER instantaneous field of view (IFOV) scan angles are defined with respect to the

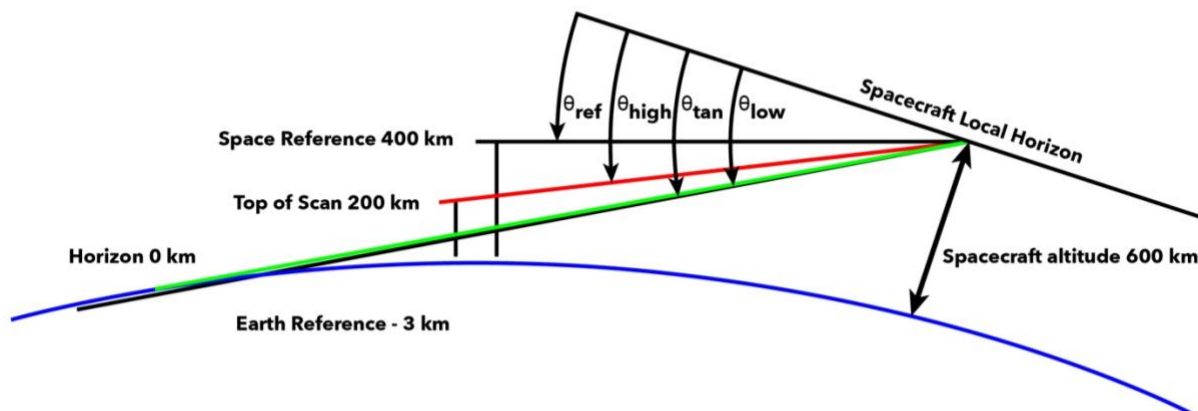287 spacecraft local horizonal as shown schematically in Figure 6.

288

289

290 **Figure 6.** Schematic sketch defining SABER scan angles relative to the spacecraft local horizon.

16

291   The SABER instrument Earth limb scan sequence is shown schematically in Figure 7

292   where the acquisition scan profile is on the left side of the figure and the adaptive scan is on the

293   right. The acquisition mode is used to locate the altitude of the CO_2 (W) layer, and only used when

294   the scanner is transitioned from the safe-hold position to scanning. The adaptive scan mode is used

295   to make scientific measurements of atmospheric emissions in the 10 SABER spectral bands. Both

296   the acquisition scan and the adaptive scan accommodate worst-case spacecraft altitude and attitude

297   variations over the mission life. The limb scan sequence is very similar to that used by the Limb

298   Infrared Monitor of the Stratosphere (LIMS) instrument that flew in the late 1970s on the Nimbus

299   VII spacecraft.

300   The width of the acquisition scan is 16.34 degrees because the bottom of the acquisition

301   scan is 26.58 degrees with respect to the spacecraft local horizon and the top is 10.24 degrees. The

302   width of the adaptive scan is 5.8 degrees because the bottom of the adaptive scan is 26.58 degrees

303   and top of the adaptive scan is 20.78 degrees. For every other adaptive scan, the scanner slews

304   rapidly to the space reference and dwells for 10 sample periods before slewing back to the top of

305   the adaptive scan. During adaptive scanning the offset is corrected based on the wide-channel CO_2

306   (W) data. The adaptive scan rate provides five samples in each 2 km vertical interval at 60 km

307   tangent height. Periodically, the scan mirror points at the IFC for 17.5 seconds.
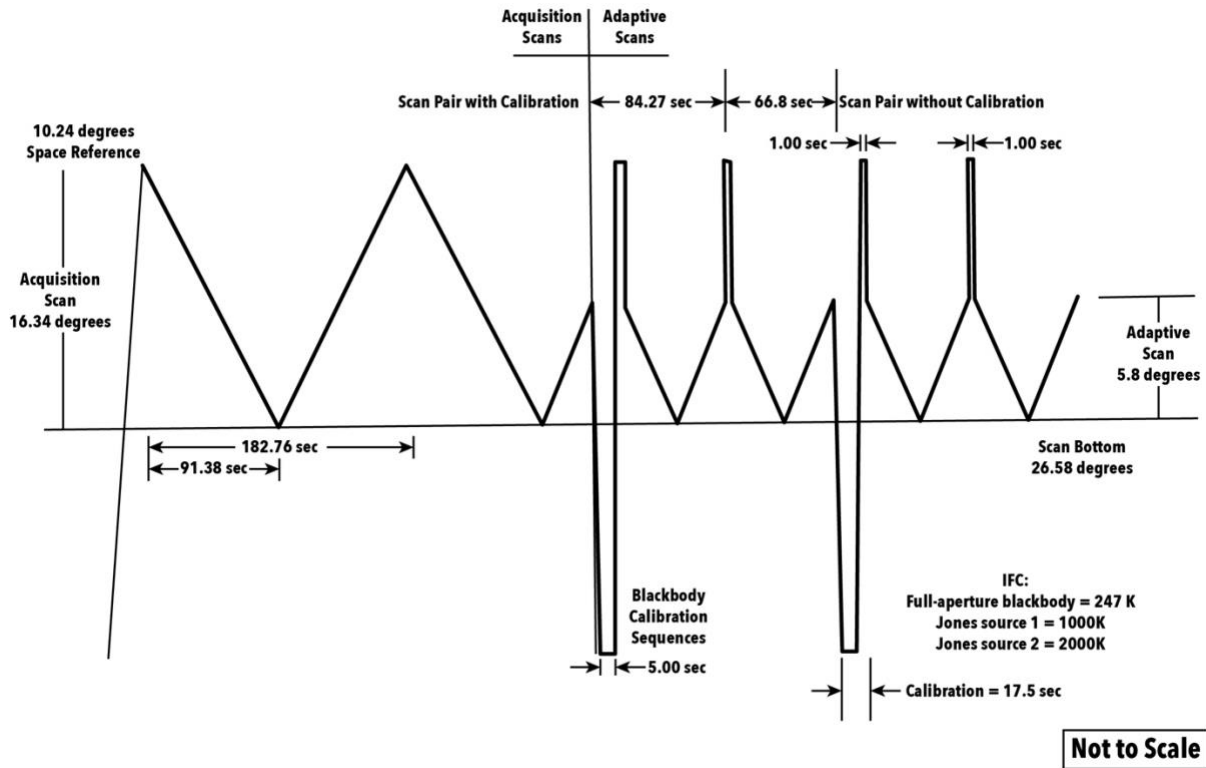
308

Figure 7 diagram labels:

Acquisition Scans | Adaptive Scans

Scan Pair with Calibration ←— 84.27 sec —→ ←— 66.8 sec —→ Scan Pair without Calibration

1.00 sec →| |← →| |← 1.00 sec

10.24 degrees
Space Reference

Acquisition
Scan
16.34 degrees

Adaptive
Scan
5.8 degrees

←———— 182.76 sec ————→
←— 91.38 sec —→

Scan Bottom
26.58 degrees

Blackbody
Calibration
Sequences

→| |← 5.00 sec

IFC:
Full-aperture blackbody = 247 K
Jones source 1 = 1000K
Jones source 2 = 2000K

→| |← Calibration = 17.5 sec

Not to Scale

Figure 7. SABER Earth limb scan sequence.

The relative locations of the 10 IFOVs on the atmosphere are shown in Figure 8. Each IFOV is nominally 2 km wide at an Earth limb tangent height of 60km and its length is as long as the optical system would allow to maximize the signal. The scan mirror translates these IFOVs up and down through the atmosphere using the acquisition or adaptive scan modes.
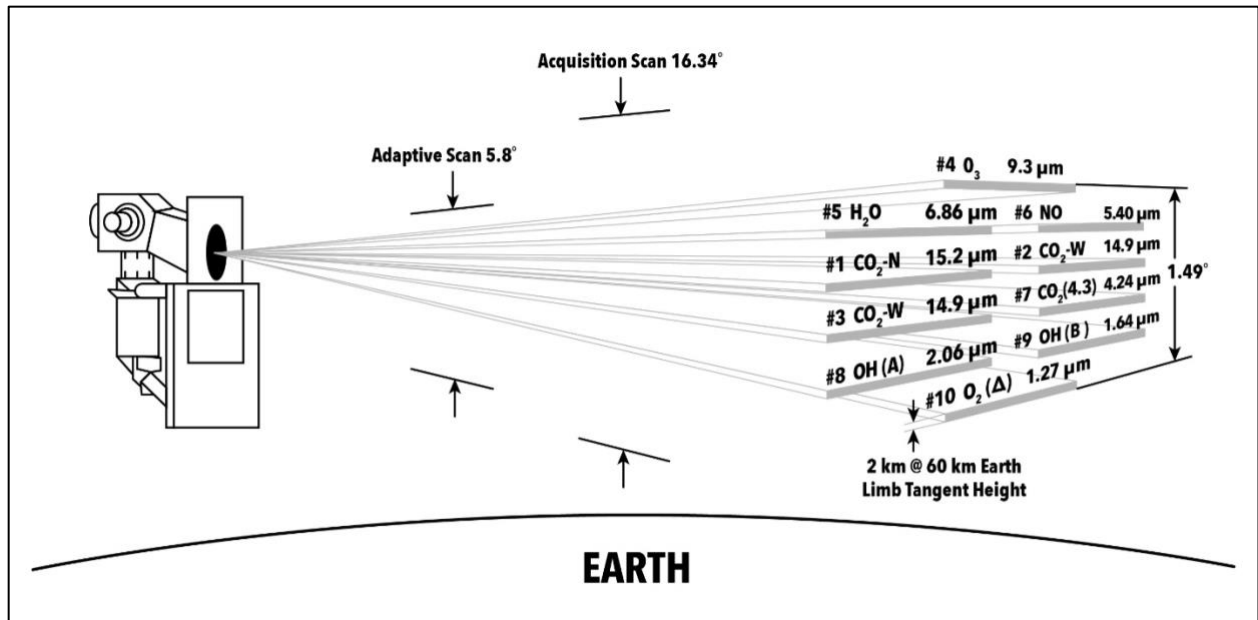
Figure 8. IFOVs of the 10 SABER detectors on the atmosphere.

2.1.1 SABER Purge and Vent System

To reduce vulnerability to water outgassing and to control particulate redistribution and contamination within the detector assembly (which is not hermetically sealed) SABER was designed with an optimized purge and vent system (*Dyer et al*., 2002) as shown in Figure 9. The purge system maintained the cleanliness and optical quality for those times when SABER was not being operated under or stored in vacuum. To make the purge system effective, dry nitrogen gas needs to be distributed uniformly into critical compartments and the escape paths must be minimized so that a slight positive pressure (4-6 Torr) can be maintained at a reasonable flow rate. This was accomplished using a purge manifold that distributed dry nitrogen to five locations: two ports in the fore-optics and scanner compartment, and one port each for the re-imager compartment, the pulse tube/thermal link compartment, and the detector. The telescope purge lines were 1/8" Teflon tubing and the FPA used 1/16" tubing to restrict the gas flow to < 3% of the total purge (nominally 0.5 standard cubic feet per meter (SCFM) at 4 psi delivery pressure). The purge

332   manifold includes a 5-µm particle filter and for each purge fitting, the telescope uses a sintered

333   metal gas snubber filter disk to provide additional filtering and eliminate stray light leaks. Once

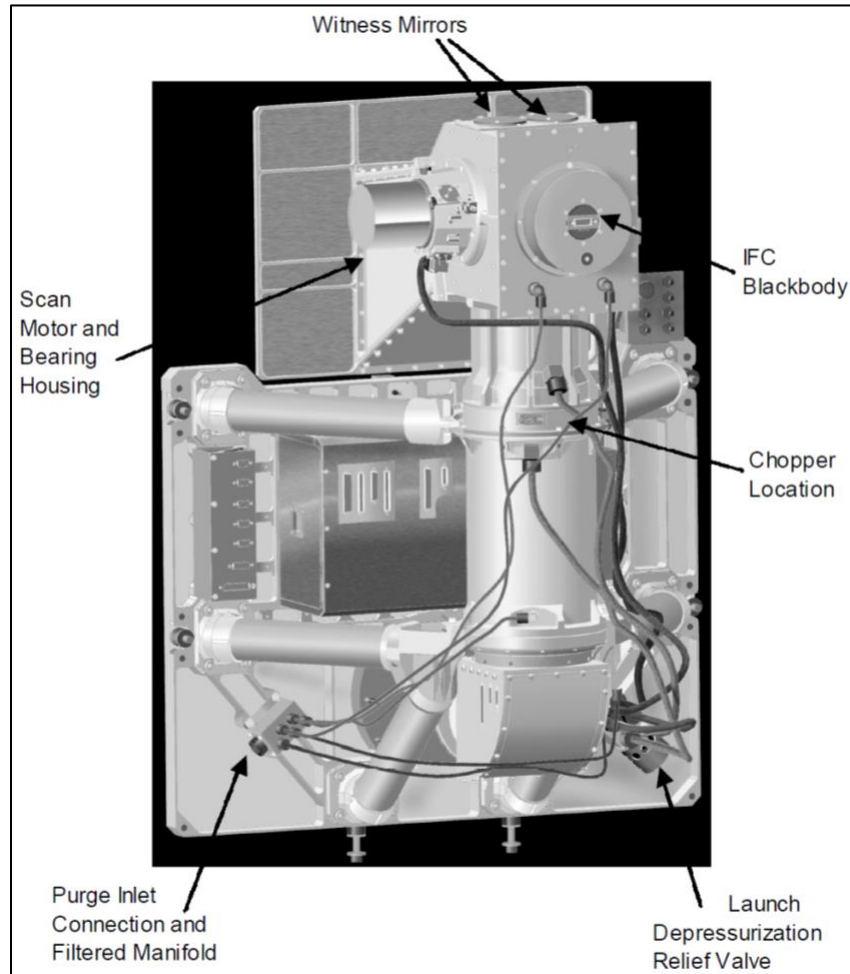334   installed, the purge system operated continuously whenever the sensor was not under vacuum.

335

336   **Figure 9.** The SABER instrument purge and vent system.

337

338   To minimize the risk from rapid launch depressurization, a very low pressure/high flow

339   relief valve was designed and tested to maintain positive pressure during purge operations and

340   control the SABER instrument depressurization vent paths during launch. The spring load on the

341   valve was adjustable to allow 0.2-0.7 scfm flow rates at 3-6 Torr pressure differential during

342   purging. However, when exposed to rapid decreases in pressure, the relief valve would open and

343   allow the SABER instrument volume to completely evacuate within 60 seconds.

344   The vent port fittings attached to the telescope used a black labyrinth that would not impede

345   gas flow but still minimized the entry of stray light. The vents were strategically located in critical

346   areas of the telescope: 1) the scanner motor and encoder which each had a vent on its body so that

347   gas flow and particulates (from the bearings) would be directed away from the optics; 2) a vent

348   port located on each side of the small chopper apertures reduced the flow of gas across the chopper

349   and reduced the possibility of damage; and 3) a vent port located on the thermal link compartment

350   directed particles from the MLI away from the detector and optics. The vent ports connected to

351   the relief valve with 3/8" Teflon tubing. The entire back of the SABER sensor was completely

352   enclosed in a 40-layer MLI blanket with a 5-mil outer layer to immunize the sensor from the

353   spacecraft thermal and outgassing environment. Since the vent valve was inside the MLI "tent",

354   purging under this configuration created a local N_2 environment outside of the telescope housing

355   as well as inside. Furthermore, the isolation afforded by the SABER thermal mechanical and

356   optical design eliminated the need for spacecraft bakeout requirements.

357   **3. SABER Instrument Level Parameters**

358   This section describes instrument level parameters including radiometric, optical, and

359   electrical in addition to SABER instrument performance.

360   Table 1 presents the spectral parameter values for each of the 10 SABER infrared channels.

361   SABER is a filter radiometer with each channel having a unique filter over its detector. The filter

362   passes infrared radiation with a defined spectral region that optimizes the ability to derive

363   temperature and constituent concentrations from the infrared radiance measurements. The filters

364   are characterized by 'cut-on' and 'cut-off' wavelengths that define the observed spectral interval.

365 There is further a central wavelength of this spectral region defined by the cut-on and cut-off. The

366 transmission of each filter is typically normalized to 1.0 at the maximum transmittance value. From

367 this, wavelengths at which the transmittance is 5% (relative to the peak transmittance) on either

368 size of the passband center is specified. The spectral specification is given in both wavelength

369 (μm) and reciprocal wavelength or wavenumbers (cm^{-1}). It is critical that the spectral filter pass

370 radiation only within the specified bandpass. For this reason, an out of band rejection ratio is

371 defined for each filter. In Table 1 the "W" and "N" on the CO_2 channels refer to 'wide' and

372 'narrow' in the sense of the spectral width of the channels. There are also two channels observing

373 emission from the hydroxyl (OH) radical labeled "A" and "B". Other channels measure infrared

374 radiation from ozone (O_3), water vapor (H_2O), nitric oxide (NO). Channel 7 measures infrared

375 radiation from CO_2 near 4.3 micrometers.

376

377 **Table 1.** SABER instrument level spectral parameter values.

Channel		Passband Center		5% Relative Cut-On		5% Relative Cut-Off		Out-Of-Band
No	Species	(cm^{-1})	(μm)	(cm^{-1})	(μm)	(cm^{-1})	(μm)	Rejection Ratio
1	CO_2 (N)	674	14.837	698	14.327	649	15.408	< 5E-04
2	CO_2 (W)	672	14.881	764	13.089	581	17.212	< 1E-04
3	CO_2 (W)	672	14.881	763	13.106	580	17.241	< 1E-04
4	O_3	1080	9.259	1146	8.726	1013	9.872	< 3E-04
5	H_2O	1468	6.812	1567	6.382	1369	7.305	< 1E-04
6	NO	1903	5.255	1944	5.144	1862	5.371	< 1E-04
7	CO_2	2348	4.259	2392	4.181	2203	4.539	< 1E-04
8	OH (A)	4830	2.07	5151	1.941	4509	2.218	< 1E-04
9	OH (B)	6078	1.645	6414	1.559	5741	1.742	< 1E-04
10	O_2	7836	1.276	7969	1.255	7704	1.298	< 1E-04

378

379 *3.1 SABER Noise Equivalent Radiance and Dynamic Range*

380 The SABER instrument level radiometric parameter values are shown in Table 2. The NER

381 values in this table were measured during ground calibration. The other parameter values are final

382 design values. The NER is the radiance value that results in a signal-to-noise ratio of unity. The

383 dynamic range is the ratio of the maximum radiance to the NER. The maximum radiance is the

384 ratio of the radiance of a 300 K blackbody (indicated in the fourth column of Table 2) to the NER

385 for channels 1 through 7. For channels 8 through 10 it is the ratio of the modeled Earth and

386 atmosphere radiance at a tangent height of -3 km to the NER.

387   The definitions of NER, dynamic range, and maximum signal are given in the footnotes to

388 Table 2. Three programable amplifiers with adjustable DC offsets follow each of the ten phase-

389 look amplifiers to make it possible to cover the required dynamic gains with a 12-bit analog to

390 digital converter (ADC). The gains of these amplifiers that achieve the required dynamic ranges

391 for each of ten channels are given in Table 2. The maximum radiance values for channels 1 through

392 7 are the radiance values of a 300K blackbody, and the maximum radiance values for channels 8

393 through 10 are modeled radiance values from the earth and atmosphere at a tangent height of -3

394 km.

395

396 **Table 2.** Instrument level radiometric parameter values.

Channel		[1,2]NER $(W/m^{-2}sr^{-1})$	300 K Radiance $(W/m^{-2}sr^{-1})$	Modeled Earth & Atmosphere Radiance $(W/m^{-2}sr^{-1})$	[3]Dynamic Range (N/A)	Programable Amplifier Gains			Gain Trip Points in ADC counts	
#	Species					High (V/V)	Medium (V/V)	Low (N/A)	High (N)	Low (N)
1	CO_2 (N)	2.45E-04	5.63E+00	2.70E+00	2.3E+04	21.1	21.1	1.0	4080	174
2	CO_2 (W)	2.84E-04	2.44E+01	9.98E+00	8.6E+04	60.0	7.7	1.0	4080	470
3	CO_2 (W)	3.32E-04	2.44E+01	9.98E+00	7.3E+04	68.6	8.3	1.0	4080	442
4	O_3	3.96E-05	9.49E+00	5.67E+00	2.4E+05	183.4	13.6	1.0	4080	269
5	H_2O	2.36E-05	5.48E+00	4.96E-01	2.3E+05	152.5	12.2	1.0	4080	294
6	NO	1.48E-06	3.63E-01	2.03E+00	2.5E+05	210.1	11.0	1.0	4080	192
7	CO_2	8.02E-07	1.48E-01	1.60E-02	1.8E+05	76.8	8.9	1.0	4080	413
8	OH (A)	1.28E-06	7.75E-05	2.48E+00	1.9E+06	1107.5	29.5	1.0	4080	110
9	OH (B)	3.33E-06	4.48E-07	4.68E+00	1.4E+06	1080.4	33.1	1.0	4080	111
10	O_2	2.49E-06	4.64E-11	2.15E+00	8.7E+05	376.3	19.6	1.0	4080	187

397 [1]Noise Equivalent Radiance (NER) is radiance value that results in a Signal-to-Noise Ratio (SNR) of unity.
398 [2]NER values are from the ground calibration.
399 [3]Dynamic Range = (Maximum Radiance)/NER
400   where (Maximum Radiance) equal radiance of 300 K blackbody for channels 1 thru 7,
401   and modeled radiance of earth and atmosphere at a tangent height of -3 km for channels 8 thru 10.
402

3.2 SABER Optical Parameters

403

404 The instrument level optical parameters with the same values for all channels are shown in

405 Table 3.

406

407 **Table 3.** SABER instrument level optical parameters that have the same value for all channels.

Parameter	Value	Units
Spacecraft Orbit Altitude at launch	625 ± 25	km
Effective Focal Length (EFFL)	200	mm
Entrance Pupil Diameter	98	mm
Central Obscuration Diameter	54	mm
Number of Secondary mirror struts	3	N/A
Total strut obscurations area	3.219	cm^2
Entrance Pupil Area	49.309	cm^2
Solid Angle Ω	0.115	
Chopper Modulation Factor	0.446	N/A
Chopping Frequency	1000	Hz
Limb Scan Mirror Jitter (1σ)	1.5	arcsec
Limb Vertical Sampling Interval	0.38	km
FOV Scan Velocity	0.179	deg/sec
Acquisition Scan	16.34	deg
Adaptive Scan Range	5.8	deg
Optical Clear Fields of View	$\pm$ 30 Horizontal, 25 Top. 55 Bottom	deg
Thermal Clear field of View	180 in all direction	deg
Ground Dry Nitrogen Purge Rate	0.5 (At 4 psi delivery pressure)	SCFM

408

409 The image of the entrance aperture, the central obscuration, and the secondary mirror

410 assembly define the optical beam that reaches the detector. The image at the Lyot stop of the outer

411 edge of the entrance aperture, which is located right in front of the primary mirror, defines the

412 outer edge of the optical beam which is focused on the detectors. The image of the secondary

413 mirror baffle at the Lyot stop defines the inner limit of this optical beam. The secondary mirror

414 which includes the secondary mirror and the secondary mirror baffle, is supported by a 3-vane (3-
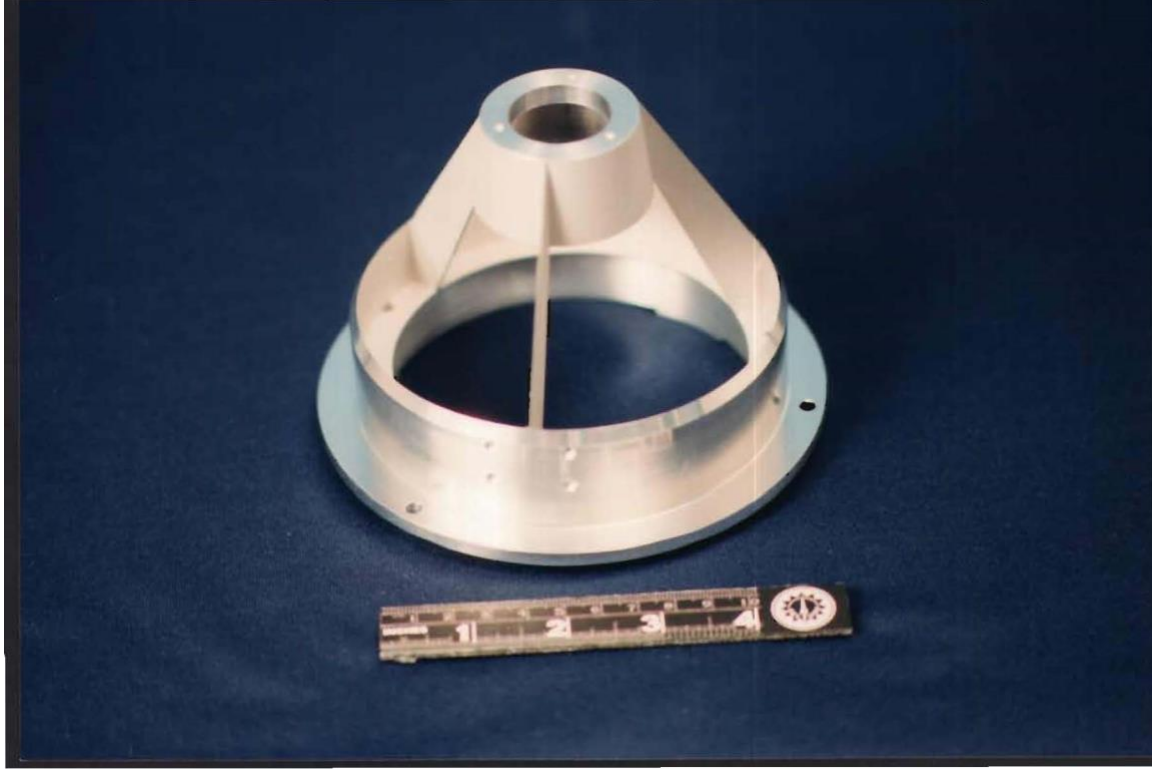
415 leg) spider (Figure 10).

416

Figure 10. Secondary mirror support and baffle.

418

419　　　　The solid angle, Ω, of the collected light beam at the detector is defined by the half angle

420　　at the detector of the image of the outer aperture edge (θ_1), and half angle at detector of inner

421　　aperture edge image (θ_2), and the fraction of the exit pupil annulus formed by the images of the

422　　outer aperture and inner aperture not obstructed by spider vanes (τ_a). The value of the solid angle

423　　for all channels is the same. The solid angle was computed using the follow equation:

424
$$\Omega = \tau_a \pi (\sin \theta_1{}^2 - \sin \theta_2{}^2) \tag{1}$$

425　　Its value, as shown in Table 3, is 0.115.

426　　　　The chopper modulation factor 0.446 is the same for all detectors and is very close to the

427　　perfect square wave modulation factor, 0.4502. Image smear in minimized by the small value of

428　　limb scan jitter. The scanning parameters are illustrated in the limb scan sequence in Figure 8

429　　above. The clear optical field of view on the spacecraft is specified to prevent glints from getting

430   into the entrance aperture. The radiators clear field of view maximize the efficiency of the

431   radiators. The SABER instrument was purged up to launch with dry gaseous nitrogen to minimize

432   contamination from water and particles. The purge system was shown previously in Figure 9.

433   The SABER instrument level optical parameters whose values are specific to each channel

434   are shown in Table 4. The vertical instantaneous IFOVs seen by each detector at a tangent viewing

435   height of 60 km are approximately 2 km. The detector areas, A_d, vary slightly from detector to

436   detector due mainly to differences in the detector's vertical dimensions. The optical throughput,

437    $A_d\Omega$, quantifies the extent of the optical beam on each detector. The parameter τ_o is the total fraction

438   of light transmitted to the detector by the product of the reflections at the five mirrors and the

439   transmittance of the filters.

440

441   **Table 4.** SABER instrument level optical parameters whose values are specific to each channel.

Channel		IFOV @ 60 km Tangent Height	Optical Throughput ($A_d\Omega$)	Transmittance (τ_o)
No	Species	(km)	(cm²sr)	(N/A)
1	CO_2 (N)	1.68	2.92E-04	0.673
2	CO_2 (W)	1.59	2.91E-04	0.820
3	CO_2 (W)	1.49	2.92E-04	0.820
4	O_3	1.97	3.38E-04	0.796
5	H_2O	1.73	3.41E-04	0.782
6	NO	1.97	3.39E-04	0.641
7	CO_2	2.12	3.37E-04	0.638
8	OH (A)	1.97	3.44E-04	0.776
9	OH (B)	1.97	3.44E-04	0.757
10	O_2	1.97	3.41E-04	0.549

442

3.3 SABER Electrical Parameters

444   The SABER instrument electrical parameters are listed in Table 5. The integration time is

445   the observation time per measurement. The signal to noise ratio (SNR)increases as the square root

446   of the integration time. The SABER instrument bandwidth is determined by 10 low-pass, 4-pole

447   Butterworth filters located in the signal processing string right after the phase-lock amplifiers. The

448   noise equivalent bandwidth (NEBW) is the bandwidth of an ideal square bandwidth that the same

449   noise as the true bandwidth. NEBW was calculated using the following equation.

450    $$NEBW = \left(\frac{\pi}{2}\right)^{\frac{1}{8}} f_{3dB} = 4.687 Hz \qquad (2)$$

451   where

452    $$f_{3dB} = 4.430 \ Hz \qquad (3)$$

453   is the 3dB bandwidth of a 4-pole Butterworth filter. The total data rate sent down to the earth is

454   extremely small; it is only 3969.7 bits/sec. The required instrument power depends chiefly on how

455   much sunlight is incident on the radiators. The amount of sunlight on the radiators is determined

456   by the β angle, the angle between the solar vector and its projection on the orbit plane.

457

458   **Table 5**. SABER instrument level electrical parameter values.

Parameter	Value	Units
Integration time	0.110	s
Noise Equivalent Bandwidth (Δf)	4.545 (1/[2x0.110 sec])	Hz
Electrical 3dB Bandwidth	4.430 (4 pole Butterworth response)	Hz
Data Sample Rate	22.727 (2.5 x Nyquist sample rate of 9.09 Hz)	Hz
Data Collection Rate	3969.7	bits/s
Instrument Power	52.64 Cold Case β=90º, 61.04 Cold Case β=0º by test	Watts
Operational Heater Power	27.16 Cold Case β=90º, 0.0 Cold Case β=0º by test	Watts
Operational Power	79.80 Cold Case β=90º, 61.04 Cold Case β=0º by test	Watts
Survival Heater Power	48.60 Cold Case β=90º, 0.0 β=0º by test	Watts
Total Peak Power	120.3 (operational cold case β=90º)	Watts
Supply Voltage	24 to 35, nominal 28	Volts
Electronic Box Size	441 (width) by 262 (height) by 192 (depth)	mm
Electronic Box Mass (Electronics Box including TRW cryocooler electronics)	7.9 ± 0.3	kg
Motherboard and Cards Mass	6.1 ± 0.3	kg
Electronic Box Dissipated Power	29.0 cold case, 29.7 hot case	watts
Maximum Junction Operating Temperature	< 373	K
Minimum Expected Operating Temperature	248	K
ΔT between Radiator and Most Distant Component	≤ 75	K
Electronic Box Interface Temperature (on orbit)	245 to 262	K
Radiation Hardness (Total Dose, no latch-up, recoverable SEU)	5	krad
Reliability	17,500	hrs

460

3.4 SABER Temperature, Mass, Size, Cleanliness, and Mission Life Parameters

The SABER instrument level temperature, mass, size, cleanliness, and mission life parameter values are shown in Table 6.

464

Table 6. SABER instrument level temperature, mass, size, cleanliness, and mission lifetime parameter values.

Parameter	Value	Units
Telescope Radiator Temperatures	209 Extreme Cold Case, 228 Extreme Hot Case	K
Telescope Average Temperatures	214 Extreme Cold Case, 237 Extreme Hot Case	K
Electronics and Cryocooler Radiator Temperature	244 Extreme Cold Case, 263 Extreme Hot Case	K
Refrigerator Mount Temperature	260 Extreme Cold Case, 278 Extreme Hot Case	K
FPA Temperature	75	K
Envelope	797 Width x 676 Depth x 1049 Height	mm
Mass	74.58 Launch Configuration, 74.07 Cover Deployed	kg
SABER Coordinate System Origin (SCSO) Location	At scan shaft center	N/A
Center of Mass about SCSO	0.43 X, 17.37 Y, 38.00 Z Launch 0.43 X, 17.26 Y, 38.24 Z Cover Deployed	cm
Moments of Inertia about SCSO at Launch	I_{xx}=20.92, I_{yy}=18.43, I_{zz}=6.218, I_{xy}= 0.168, I_{yz}=6.606, I_{xz}=0.390	kg m^2
Moments of Inertia about SCSO after Cover Deployed	I_{xx}=20.83, I_{yy}=18.41, I_{zz}=6.140, I_{xy}= 0.168, I_{yz}=6.581, I_{xz}=0.390	kg m^2
Loads Environment	15.5 Max of Launch &Testing Loads (Driven by Sine Burst Test)	g
Vibration Environment	8.5 (TIMED proto-flight level Environmental Spec for 72 kg mass	g rms
Minimum Frequency Stiffness	49.13 Hz (thrust axis, 40.31 Hz (x axis), 42.04 Hz (y axis)	Hz
Exterior Cleanliness Level	750	N/A
Mission Life	2 required, but SABER still taking excellent data after 21	years

467

3.5 SABER Stray Light Parameters

SABER is an instrument that measures infrared emission from the atmosphere by viewing the limb of the Earth. As shown previously in Figure 1, SABER limb radiance measurements cover a large dynamic range of several orders of magnitude, depending on channel. This fact places very stringent requirements on the stray light rejection properties of the SABER instrument. As noted above, the IFOV of SABER is 2 km. Light entering the instrument and falling on the detector from

474 outside this IFOV is considered stray light. The entrance aperture of SABER is illuminated by the

475 entire atmosphere below the tangent point. Because of the rapid increase of radiance with

476 decreasing tangent altitude, SABER's optical system must be capable of rejecting several orders

477 of magnitude of radiance emitted within just a few degrees below the observed tangent height. For

478 the CO_2 (W) channel (which is used to derive temperature) shown previously in Figure 1, 1% of

479 the radiance from 45 km tangent height is equal to the radiance at 80 km tangent height. For

480 SABER and all thermal emission limb sounders, rejection of off-axis (out of field) radiation is

481 paramount.

482   SABER's optical system was designed specifically to have extremely high rejection of off-

483 axis light. Initial analysis of SABER's stray light performance is reported by *Stauder et al.* (1995).

484 During the development of the instrument, a stray light analysis was performed using a non-

485 sequential ray tracing Zemax model of SABER and an SDL software program to compute the

486 Normalized Detector Irradiance (NDI). NDI is a fundamental measure of an instrument's

487 sensitivity to off axis stray light. It is the ratio of irradiance reaching the detector to that incident

488 on the entrance port to the instrument, as a function of off-axis angle, and is computed using the

489 following equation:

490 $$NDI(\theta) = \frac{Detector\ Irradiance\ (\theta)}{Port\ Irradiance(\theta)}$$ (4)

491 where θ is the angle that the source beam makes with the telescope baffle centerline. The point

492 source is assumed to be at an infinite distance and is represented by a collimated ray bundle that

493 fills the baffle entrance aperture. The computed instrument NDI values for each SABER channel

494 at specified tangent heights are illustrated in Table 7 and plotted in Figure 11. For the example of

495 the CO_2 (W) channel given above, the 45 km tangent height is approximately 1 degree in angle

496   below the 80 km tangent height from SABER's orbit altitude. Table 7 shows an NDI of 0.17% for

497   the CO_2(W) channel at 1 degree, illustrating the exceptional off-axis rejection of the instrument.

498

499   **Table 7**. SABER instrument NDI as a function of off-axis angle (q) in degrees.

| Channel		Center Wave-length	NER	Tangent Height h_{tan}	NDI							
					Off-Axis Angle (degrees)							
#	Species	(mm)	(W/[cm²sr])	(km)	1	5	10	17	20	35	55	75
1	CO_2 (N)	14.837	2.45E-04	70	1.7E-03	2.6E-05	2.2E-06	7.9E-09	6.7E-11	9.8E-12	2.7E-12	8.4E-13
2	CO_2 (W)	14.881	2.84E-04	70	1.7E-03	2.6E-05	2.2E-06	7.8E-09	6.7E-11	9.8E-12	2.7E-12	8.4E-13
3	CO_2 (W)	14.881	3.32E-04	70	2.8E-03	2.4E-05	2.0E-06	7.3E-09	6.4E-11	9.5E-12	2.7E-12	8.2E-13
4	O_3	9.259	3.96E-05	70	3.4E-04	9.5E-06	8.6E-07	1.4E-10	2.3E-11	6.5E-12	2.0E-12	3.6E-13
5	H_2O	6.812	2.36E-05	70	4.3E-04	9.0E-06	6.7E-07	6.4E-11	1.7E-11	4.5E-12	1.4E-12	3.3E-13
6	NO	5.255	1.48E-06	100	4.7E-04	1.4E-05	1.0E-06	1.5E-08	2.5E-11	9.4E-12	3.0E-12	2.7E-13
7	CO_2	4.259	8.02E-07	80	2.1E-03	2.1E-05	1.3E-06	1.8E-08	2.9E-11	1.1E-11	3.6E-12	3.6E-13
8	OH (A)	2.07	1.28E-06	87	3.6E-04	1.7E-06	1.4E-07	1.8E-10	2.0E-12	9.0E-13	3.2E-13	1.8E-14
9	OH (B)	1.645	3.33E-06	87	7.4E-04	2.6E-06	2.2E-07	2.3E-10	2.4E-12	1.0E-12	3.8E-13	2.3E-14
10	O_2	1.276	2.49E-06	70	4.0E-03	5.4E-06	4.1E-07	2.3E-11	3.1E-12	1.4E-12	5.3E-13	3.4E-14

500

501
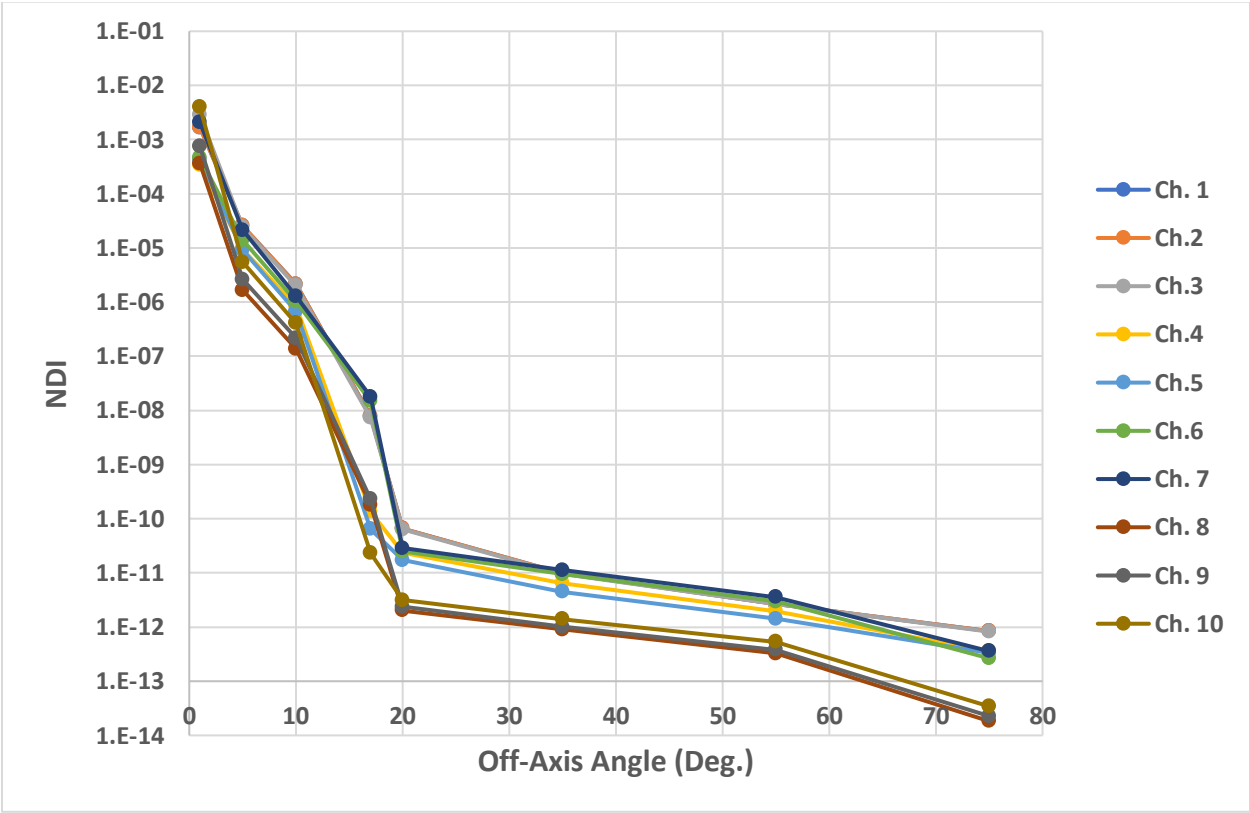
502   **Figure 11.** SABER instrument NDI plots versus off-axis angle.

503

504 The product of the NDI curve and the radiance from the Earth and atmosphere is integrated

505 over all angles in the hemisphere of angles looking out from SABER to compute the Non-Rejected

506 Radiance (NRR) at various tangent heights for each SABER channel. Two figures of merit are

507 developed to assess SABER's off-axis rejection performance. The first is the ratio of the NRR to

508 NER reported earlier in Table 2 and listed in Table 8 in the column labeled (NRR/NER). This

509 column demonstrates that the SABER non-rejected radiance at the indicated tangent altitudes is

510 substantially less than the instrument noise, sometimes by several orders of magnitude.

511 The second figure of merit is the ratio of the limb radiance at a given tangent height to the

512 NRR. This ratio, listed in the right-most column of Table 8, is the "signal-to-stray-light ratio." As

513 seen in Table 8, it ranges from 120 to over 628,000 depending on channel and tangent height. Both

514 figures of merit indicate that SABER has excellent stray light rejection ability. Operational

515 experience and the SABER data quality as reflected in more than 2200 peer-reviewed publications

516 confirms this excellent optical performance.

517

518 **Table 8**. SABER non-rejected radiance metrics

Channel		Center Wave-length	NER	Tangent Height h_{tan}	NRR	NRR/NER	Radiance (h_{tan})	Radiance(h_{tan}) /NRR
#	Species	(mm)	(Wm^{-2}sr^{-1})	(km)	(Wm^{-2}sr^{-1})	(N/A)	(Wm^{-2}sr^{-1})	(N/A)
1	CO_2 (N)	14.837	2.45E-04	70	5.113E-05	2.090E-01	2.326E-02	455
2	CO_2 (W)	14.881	2.84E-04	70	1.854E-04	6.530E-01	3.562E-02	192
3	CO_2 (W)	14.881	3.32E-04	70	2.980E-04	8.980E-01	3.562E-02	120
4	O_3	9.259	3.96E-05	70	1.318E-09	3.327E-05	2.645E-04	200784
5	H_2O	6.812	2.36E-05	70	1.204E-09	5.104E-05	2.638E-04	219001
6	NO	5.255	1.48E-06	100	1.117E-07	7.600E-02	1.093E-04	978
7	CO_2	4.259	8.02E-07	80	2.880E-07	3.590E-01	2.294E-04	796
8	OH (A)	2.07	1.28E-06	87	9.169E-10	7.163E-04	5.766E-04	628895
9	OH (B)	1.645	3.60E-08	87	4.159E-09	1.160E-01	8.541E-04	205335
10	O_2	1.276	2.49E-06	70	1.481E-08	5.948E-03	4.095E-04	27649

519

4. Major Components of the SABER Instrument

4.1 SABER In-Flight Calibrator

The SABER IFC consists of a full-aperture black body and three partial-aperture Jones sources (items E and F in Figure 2). The full-aperture body is used for the long-wavelength channels numbered 1 through 6, and the Jones source calibrators are used for the short-wavelength channels numbered 7 through 10. The full-aperture blackbody is shown in Figure 12(a) and one of the three tungsten-filament Jones sources, before it is embedded in the full-aperture blackbody, is shown in Figure 12(b). After embedding, two of the three Jones sources can be seen as white glints in Figure 12(a).
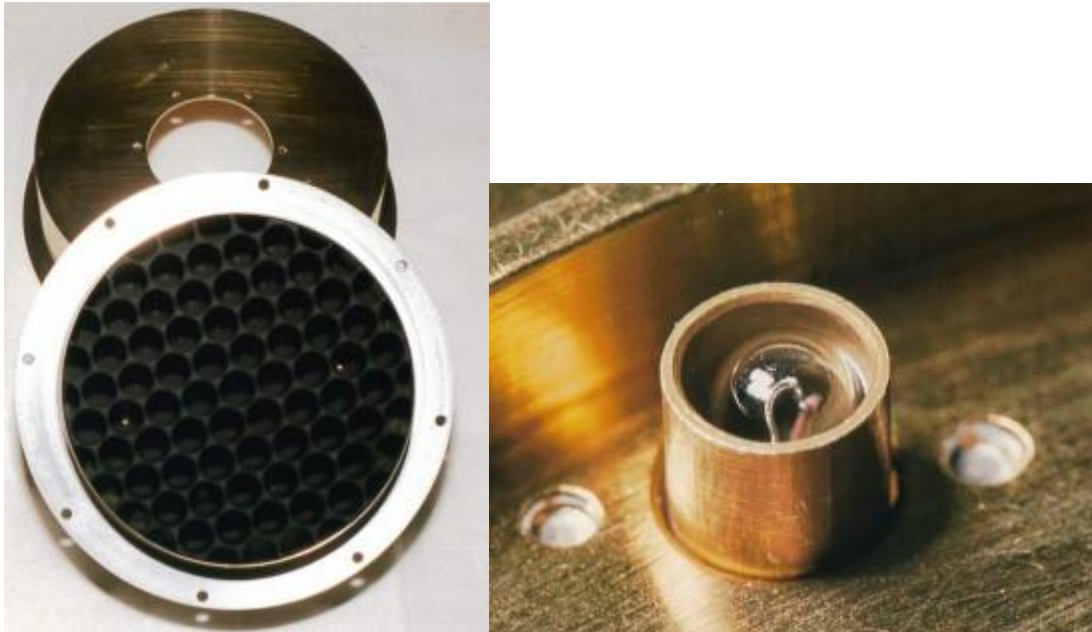
Figure 12. (a, left image) Full aperture blackbody, (b, right image) one of three tungsten-filament Jones sources before being embedded in the full-aperture blackbody.

534 *4.2 Entrance Aperture Cover*

535   The SABER entrance aperture cover, its wax actuator pin puller, and two removable

536 witness mirror covers are shown in Figure 13. These witness mirrors, which were removed and

537 replaced by covers before launch, were used to monitor contamination during SABER integration,

538 testing, storage, shipping, and TIMED launch preparations. The SABER aperture cover protected

539 the inside of the SABER instrument from contamination during SABER integration, testing,

540 storage, shipping, launch preparations, and during the maximum outgassing period at the start of

541 the mission. The SABER cover was ejected by a spring after the wax actuator pulled the retaining

542 pin. At the time of when TIMED was launched, it was still acceptable to eject instrument covers

543 without consideration of the implications for space debris. The entrance aperture cover is the item

544 labeled X in Figure 2.

545
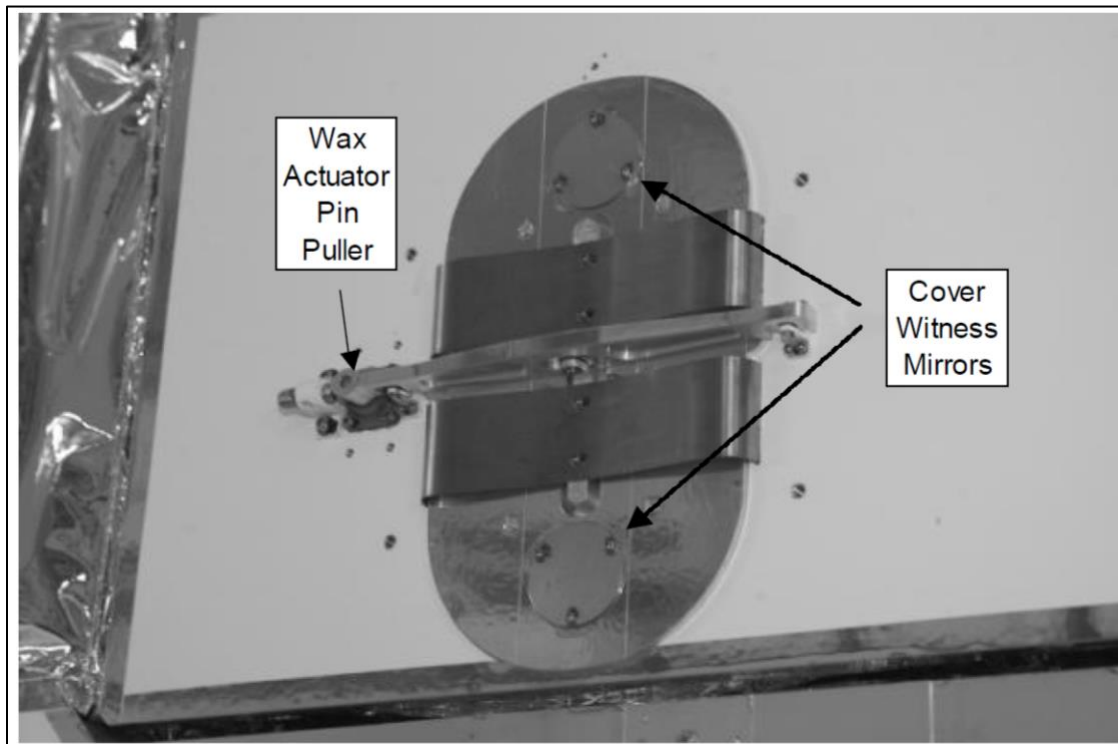
546 **Figure 13.** SABER aperture cover with its wax actuator pin puller and removable witness mirrors.

547

4.3 Fore-Optics Baffle Assemblies

The fore-optics baffle assembly, which provides baffling before the scan mirror, is shown in Figure 14 with its top removed. The baffle assembly is indicated as item B in Figure 2, located in the optical train between the optics radiator and the scan mirror. After painting, the baffle blades and baffle tips were wiped clean to minimize the baffle tip radius and hence minimize scattered light from the baffle tips. The number of baffle blades was made just large enough to satisfy the two-bounce rule for light in the baffle cavities.
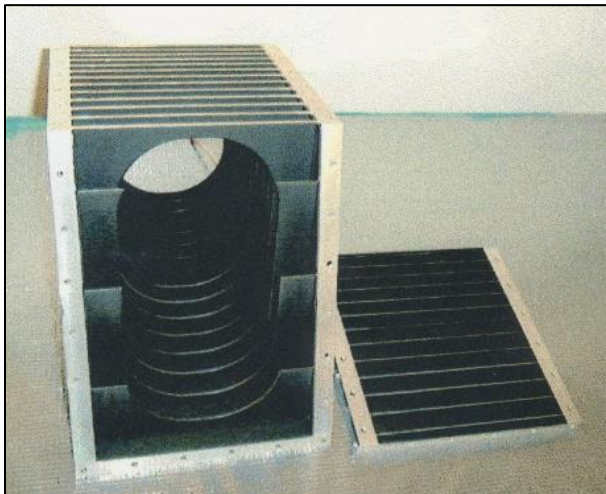
Figure 14. Fore-optics baffle assembly.

The baffle surrounding the Ritchey-Chrétien telescope is a cylindrical baffle with its entrance port at an angle to prevent it from blocking needed rays on their way to the scan mirror. This baffle is shown below in Figure 15 and surrounds mirrors M1 and M2 (Items H and J in Figure 2). A schematic drawing of this baffle can be seen in Figure 5, which also shows a schematic sketch of the fore-optics baffle.

564
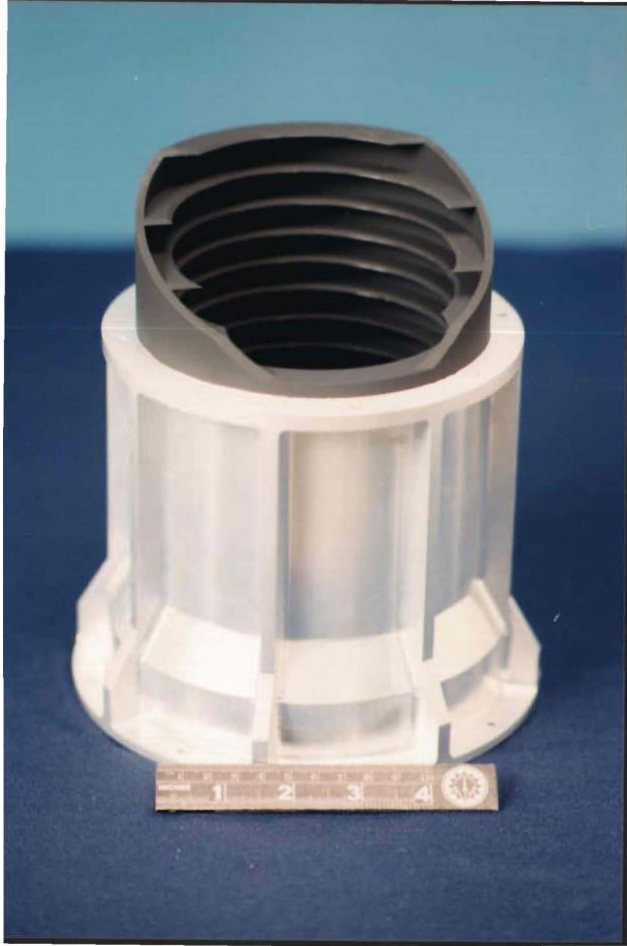
Figure 15. SABER main baffle assembly.

566

4.4 Encoder/Motor Assembly

The encoder/motor/bearing assembly is the cylindrical assembly mounted on the side of the baffle identified previously in Figure 9. This assembly is the black cylinder in the Figure 4 photograph. The parameter values of the encoder/motor assembly are given in Table 9. The encoder/motor/bearing assembly rotates the scan mirror and measures the scan mirror angle. The center of rotation is on the front surface of the scan mirror on the vertical centerline of this mirror. The ion-coated bearing lubrication is one of the most critical parameters because this mirror must rotate smoothly and easily when the bearing temperature is in the 215 to 250 K range. Periodically, the mirror is rotated past its operational limits to push any lubrication build up on the bearing races

576   past the operational rotation limits. One of the most important pointing parameters for mapping

577   the radiance versus tangent height is the encoder accuracy of 25 µradians rms (5.2 arc seconds).

578

579   **Table 9**. Encoder motor assembly parameter values.

Parameter	Value	Units
Total Rotation Travel (stop to stop)	84.4	deg
Maximum Rotor Rotational Rate	14.3	deg/sec
Pointing Accuracy	6	arcsec
Pointing Precision	0.088	deg
Moment of Inertia (Includes inertia of mirror and shaft)	6112	kg mm^2
Bearing Lubrication	Ion-coated lead	N/A
Mass	1.85	Kg
Friction Torque (Cogging and Bearing)	0.86	kg-mm
Motor Type	Brushless 3 phase DC	N/A
Number of Motor Poles	12	N/A
Motor Commutation	Hall Effect Sensors	N/A
Motor DC Resistance @ 25ºC	$10.8 \pm 10\%$	ohms
Motor Inductance	$4.5 \pm 30\%$	mH
Voltage @ 32.55 oz-in (25ºC)	25.0 nominal	volts
Torque Sensitivity	$15.1 \pm 20\%$	kg-mm/amp
Back EMF	$0.148 \pm 10\%$	volts/rad/sec
Motor Winding Isolation	$> 100, < 100$	MΩ, pF
Motor Constant	4.623	kg-mm/vw
Encoder Outputs	Quadrature w/zero ref	N/A
Encoder Cycles per Channel/Revolution	262,144 (2^{18})	N/A
Encoder Accuracy (over 360º rotation)	25	µrad rms
Signal Minimum Level (RS422)	2	volts pk to pk
Motor Power	0.7	watts
Encoder Power	2.1	watts
Non-Operating Temperature Range	208 to 333	K
Operating Temperature Range	215 to 250	K
ΔT at Encoder Mount to Baffle	5	K
Design Life Total Scan Cycles	3.8E6 (3 years)	N/A

580

581   *4.5 Mirrors*

582   The SABER optical system has five mirrors: the scan mirror; mirrors M1 and M2, which

583   constitute a Ritchey-Chrétien telescope that focuses the input light on the chopper; and M3 and

584   M4, which constitute a clamshell re-imager that reimages the chopper holes onto the filters and

585   detectors. The locations of these mirrors in the SABER optical train can be seen in Figure 2 as

586   items J, H, M, and L, respectively.

36

All the mirrors have aluminum mirror substrates that were thermal cycled between room temperature and liquid nitrogen temperatures to minimize residue internal stress. The mirror substrates have a 6:1 diameter to thickness aspect ratio and lapped, flexible three-point mounting pads to minimize reflected wavefront error. The aluminum substrates were diamond turned and polished to near final optical figure, then the front and back of the mirror substrates were coated with electroless nickel. The thickness of the nickel on the back surface was slightly less than on the front surface so that the thicknesses of the front and back nickel coating were nearly equal after polishing. Only a narrow strip near the front of each mirror is nickel coated so that mirror deformation due to hoop stress when the mirror is coated is minimized. This thin strip can be seen on the edges of the primary mirror and the tertiary mirror later in this document in Figure 16 (Section 4.5.1) and Figure 23 (Section 4.9), respectively. After nickel coating, the mirrors were super polished to their final optical figure. Super polishing minimizes the bi-directional reflectance distribution (BRDF) function and hence minimizes reflected stray light. Finally, the mirrors were coated with a very thin layer of gold to maximize reflectance at the SABER passband wavelengths and minimize thermal emissions.

4.5.1 Scan Mirror

The scan mirror parameters are listed in Table 10 and indicated as item C in Figure 2. The most important scan mirror parameters are the BRDF and peak-to-valley surface error. The BRDF of the scan mirror is exceptional good; that is, it is small and decreases rapidly with increasing angle from the reflecting surface normal. This was achieved by applying an electroless nickel coating over an aluminum substrate. The nickel coating allowed super-polishing of the mirror to a rms surface roughness of approximately 10 Angstroms, which results in these good BRDF values. After super-polishing, this mirror was coated with electrolytic gold to produce the high reflectance

value given in this table for the total infrared spectral region measured. Electrolytic gold scatters

less than vacuum deposited gold. The peak-to-valley surface error at the 215 to 250 K operational

temperature of the scan mirror was achieved by making the ratio of the maximum length across

the reflected surface of the mirror to the thickness equal to 6 to 1 and by also nickel coating the

back surface of the scan mirror with same thickness of nickel. This relatively large aspect ratio

incurs a mass penalty. Nickel coating the front and back surface with the same thickness of nickel

and making the coating as thin as possible minimizes mirror bending at the cryogenic temperatures.

The distance the nickel coating extends around the mirror edge is minimized to minimize hoop

stress when this mirror is cooled. All the SABER mirrors are fabricated using the procedures

described above for the scan mirror.

Table 10. Scan mirror parameter values.

Parameter	Value	Units
Material	Gold on 0.003" thick nickel on aluminum substrate	N/A
Optical Surface Figure	Plane	N/A
Size	157.256 by 110.752 oval	mm
Peak-to-Valley Surface Error @ 300 K	0.197	633 nm waves
BRDF	$2.10\text{E-}3/\theta^{2.54}$ @ 10.6 µm $1.12\text{E-}2/\theta^{2.88}$ @13.39 µm $6.14\text{E-}4/\theta^{2.06}$ @ 1.2 µm	steradian^{-1}
ΔT across mirror	$\leq$2	K
Reflectance	0.98	NA
Mass (measured)	0.86	kg
Mass of Scan Mirror Shaft Assembly (includes light trap, mirror, mirror counterbalance)	2.13	kg

4.5.2 Primary Mirror

The primary mirror, M1, is shown in Figure 16. The features that appear to be on the surface

in this photo are images of the area surrounding the mirror when this photo was taken. The hole in

the center of this mirror is to mount the primary inner conical baffle that is shown in Figure 17.

627   After painting and while the paint was still wet, the baffle blade edges were wiped clean of paint

628   as can be seen in Figure 17. This wiping procedure prevents the large amount of scattered light

629   that would result from a ball of paint on the baffle edge. Primary mirror parameter values are given

630   in Table 11. The primary mirror is fabricated using the same procedure described above for the

631   scan mirror to minimize its BRDF and its peak-to-valley surface error. The Ritchey-Chrétien

632   telescope, which consists of M1 and M2, corrects both spherical aberration and coma by using

633   hyperbolic mirrors for both the primary and secondary mirrors. Its primary mirror optical surface

634   is slightly flatter than the parabolic primary mirror used in the classical Cassegrain telescope. The

635   secondary mirror of the classical Cassegrain telescope is hyperbolic like the Ritchey-Chrétien

636   telescope.

637

638   **Figure 16.** SABER Primary mirror M1.

639

640
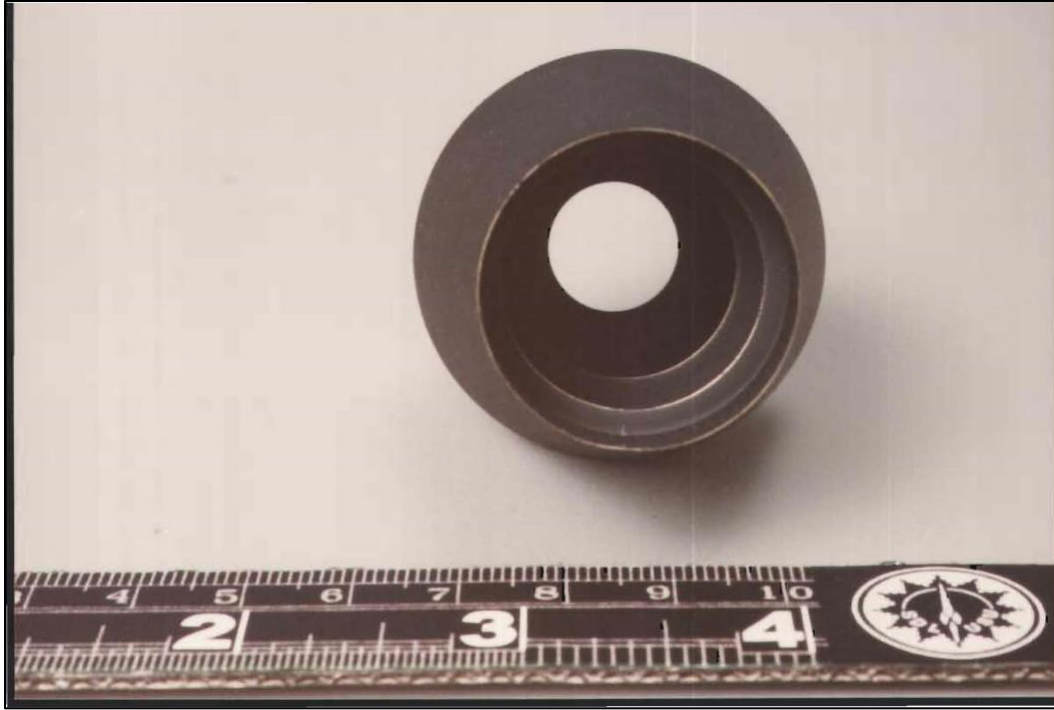
Figure 17. Primary mirror inner-conic baffle.

642

Table 11. Primary mirror parameter values

Parameter	Value	Units
Material	Gold on 0.003" thick nickel on aluminum substrate	N/A
Radius of Curvature	225.000 concave	mm
Conic Constant	-1.15149 hyperboloid	mm
Outer Diameter	106	mm
Inner Diameter	48.006	mm
Peak-to-Valley Surface Error @ 300 K	0.23	633 nm waves
BRDF (θ is the angle off specular expressed in degrees)	$9.73E\text{-}5/\theta^{1.83}$ @ 10.6 µm $2.42E\text{-}3/\theta^{2.88}$ @ 3.39 µm $2.42E\text{-}3/\theta^{2.03}$ @ 1.2 µm	steradian^{-1}
Reflectance	0.98	N/A
ΔT across mirror	≤ 2	K
Mass	0.39	kg

644

4.5.3 Secondary Mirror, Secondary-Mirror Spider, and Secondary-Mirror Baffle

A photograph of the secondary-mirror support was shown previously in Figure 10. The

secondary mirror support and baffle were fabricated as one piece using a plunge electrical

discharge machining (EDM) technique. The relatively rough EDM finish made good diffuse

40

649 surfaces. The support vanes are beveled in the direction of the rays so only the baffle edges nearest

650 the primary mirror can be seen at the Lyot stop. The Ritchey-Chrétien telescope, whose optical

651 elements are the primary and secondary mirrors, was focused by means of a planar shim between

652 the top of the second spider and the secondary mirror mounting plate.

653   The assembly procedure to install the secondary mirror was to first lay a nominal thickness

654 ring shim on the top of the support and then insert secondary mirror mounting feet through the

655 hole in the top of the support, bolt these feet to a mounting plate, and finally bolt the mounting

656 plate to the top of the support. The focus location and image quality of the M1-M2 pair was

657 checked interferometrically. The thickness of the shim and the decenter of the secondary mirror

658 relative to the primary mirror was iterated until the focus location and image quality requirements

659 were satisfactory.

660   Secondary mirror parameters are given in Table 12. The secondary mirror is fabricated

661 using than same procedures described above for the scan mirror to minimize its BRDF and its

662 peak-to-valley surface error. The optical surface of this mirror has a hyperbolic shape that is

663 defined by the values of the conic constant and the radius of curvature. The hyperbolic shape

664 slightly flattens the edge of the mirror surface compared to a spherical shape. The secondary mirror

665 is more hyperbolic than the primary mirror. The secondary mirror together with the primary mirror

666 form a Ritchey-Chretien telescope, which has zero spherical aberration and zero coma.

667

668

669

670

671

672 **Table 12**. Secondary mirror parameter values

Parameter	Value	Units
Material	Gold on 0.003" thick nickel on aluminum substrate	N/A
Radius of Curvature	120.000 convex	mm
Conic Constant	-6.62063 hyperboloid	mm
Outer Diameter	40.5	mm
Peak-to-Valley Surface Error @ 300 K	0.0817	633 nm waves
BRDF (θ is the angle off specular expressed in degrees)	$2.44\text{E-}3/\theta^{3.01}$ @ 10.6 µm $1.86\text{E-}3/\theta^{2.88l}$ @ 3.39 µm $6.14\text{E-}4/\theta^{2.06}$ @ 1.2 µm	steradian^{-1}
Reflectance	0.98	N/A
Mass (measured)	0.38	kg

673

4.5.4 Tertiary and Quaternary Mirrors

675   The tertiary and quaternary mirror pair form a clamshell re-imager optical system. After

676 light passes through the chopper, it passes through a hole in the quaternary mirror and is reflected

677 by the tertiary mirror back to the quaternary mirror that then reflects it to the FPA. The parameter

678 values of the tertiary and quaternary mirror or given in Table 13 and Table 14, respectively. The

679 tertiary mirror is fabricated using than same procedures described above for the scan mirror to

680 minimize its BRDF and its peak-to-valley surface error. The tertiary and quaternary mirrors form

681 a clamshell re-imaging system. Together they re-image the focus of the Ritchey-Chretien, which

682 is located at the tuning fork chopper, at the detector. The tertiary mirror is hyperbolic with an

683 optical surface flatter than a sphere and even a parabola. The quaternary mirror is an oblate

684 ellipsoid with the ellipse foci on opposite sides of the optical axis which makes the optical surface

685 look like a doorknob or the top of a spinning planet.

686

687

688

689

690   **Table 13**. Tertiary mirror parameter values.

Parameter	Value	Units
Material	Gold on 0.003" thick nickel on aluminum substrate	N/A
Radius of Curvature	1050.000 concave	mm
Conic Constant	-6.62063 hyperboloid	mm
Outer Diameter	127.000	mm
Inner Diameter	23.978	mm
Peak-to-Valley Surface Error @ 300 K	0.153	633 nm waves
Reflectance	0.98	N/A
Mass (measured)	0.76	kg

691

692   **Table 14**. Quaternary mirror parameter values.

Parameter	Value	Units
Material	Gold on 0.003" thick nickel on aluminum substrate	N/A
Radius of Curvature	384.407 concave	mm
Conic Constant	0.3910 oblate ellipsoid	mm
Outer Diameter	165.000	mm
Inner Diameter	37.998	mm
Peak-to-Valley Surface Error @ 300 K	0.231	633 nm waves
Reflectance	0.98	N/A
Mass (measured)	1.55	kg

693

694   *4.6 SABER Optical Chopper*

695   The SABER optical chopper (Figure 18) is located at the focus of the Ritchey-Chrétien

696   telescope. Its position in the optical train is shown as item K of Figure 2. The SABER chopper is

697   a "picket-fence" chopper, with two shutters that in principle function like two translating parallel

698   picket fences. This design amplitude modulates the light in each of the 10 IFOVs while requiring

699   only small mechanical translations of the chopper blades. This small motion maximizes chopper

700   reliability and makes it possible to chop at 1000 Hz, which is well above the 1/f noise knee of the

701   photoconductive HgCdTe detectors used for channel numbers 1 through 5. The SABER chopper

702   was made by TFR Laboratories Inc, which is now out of business. This chopper provides a nearly

703   square wave chopping of the light collected on each of SABER's 10 detectors. The chopper

704   efficiency is 0.446, which is very close to the maximum possible value of 0.4502 for a true square-

705   wave chop.

43

706   As can be seen in Figure 18, each of the chopped areas is half open at rest. The chopper

707   blades are gold coated so they have an infrared emissivity < 0.05, which minimizes thermal

708   emissions from the chopper shutters. The chopper has one set of coils to drive the chopper and one

709   set of coils to produce the reference for synchronous demodulation. The chopper operating

710   temperature is 215 K for the cold case and 240 K for the hot case. The chopper produces a

711   mechanical disturbance of 0.002 lb-ft and its measured mass is 0.095 kg.

712

713
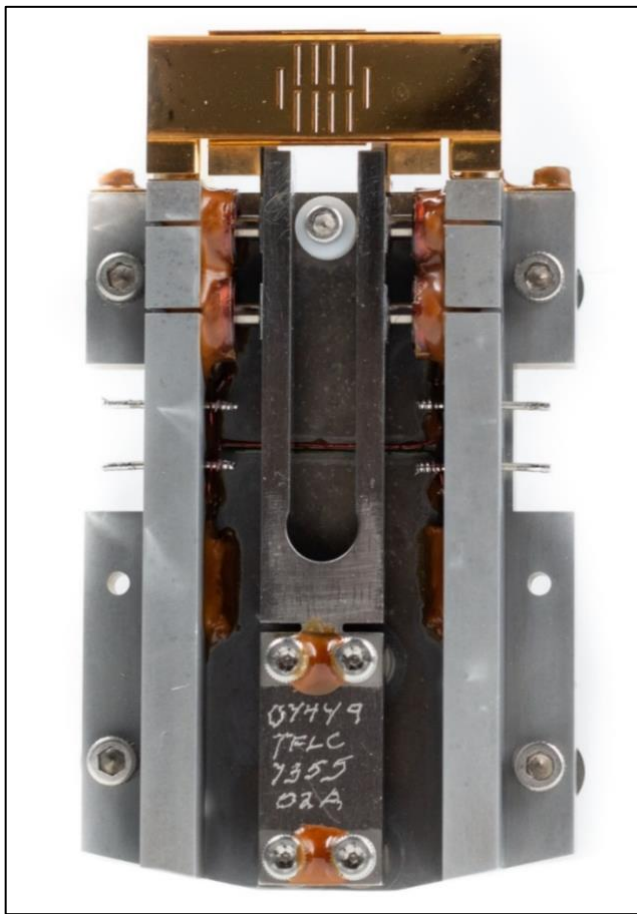
714   **Figure 18.** The SABER "picket-fence" chopper

715

4.7 SABER Focal Plane Array (FPA)

717   The SABER FPA consists of a detector array and filter array located inside the detector

718   assembly and a Lyot mounted on top of the detector assembly. The filter assembly was designed

719   and fabricated by Optical Coating Laboratory (OCLI; now VIAVI Solutions Inc.). The detector

720   array was designed and fabricated by E&G Optoelectronics (now Teledyne Judson Technologies;

721   TJT). SDL designed and fabricated the Lyot stop. The focal plane assembly is indicated as item O

722   in Figure 2.

723   Photoconductive (PC) detectors are used for the long-wavelength detector channels

724   (channels 1 through 5) and photovoltaic (PV) for the short-wavelength detector channels. Table

725   15 and Table 16 show the parameter values for the PC and PV detectors, respectively. All

726   parameter values are at the 1000 Hz SABER chopping frequency. D* is the detector specific

727   detectivity.

728   **Table 15**. SABER photoconductive (PC) detector parameter values.

Channel		Detector Material	Detector Resistance @296K	Detector Resistance @75K	Bias Current	Bias Power	Noise @1kHz	Average Responsivity	Average D* @1kHz
Number	Species								
			(Ω)	(Ω)	(mA)	(mW)	(μV/rtHz)	(V/W)	(cm$\sqrt{Hz}$/W)
1	CO_2(N)	HgCdTe	249	699	1.5	1.6	12.07	1.9E+04	7.53E+10
2	CO_2(W)	HgCdTe	233	606	1.5	1.4	11.57	1.4E+04	5.76E+10
3	CO_2(W)	HgCdTe	269	681	1.5	1.5	13.1	1.5E+04	5.44E+10
4	O_3	HgCdTe	530	1274	1.0	1.0	7.46	1.4E+05	9.19E+11
5	H_2O	HgCdTe	1209	2563	1.0	1.0	9.56	1.2E+05	6.50E+11

729

730   **Table 16.** SABER photovoltaic (PV) detector parameter values.

Channel		Detector Material	Feedback Resistance	JFET Pair Bias Power	Noise @1kHz	Average Responsivity	Average D* @1kHz
Number	Species		(Ω)	(mW)	(μV/rtHz)	(A/W)	(cm$\sqrt{Hz}$/W)
6	NO	InSb	6.28E+07	3.2	0.69	3.69	1.8E+13
7	CO_2	InSb	7.10E+08	3.3	0.44	2.89	2.5E+14
8	OH (A)	InSb	1.49E+08	3.3	0.22	1.74	6.3E+13
9	OH (B)	InSb	9.06E+07	3.3	0.55	1.06	9.3E+12
10	O_2	InGaAs	9.56E+07	3.3	0.21	0.92	2.3E+13

731

732   The spectral parameters of the SABER filters are given in Table 17. These filters are

733 mounted on top of the detectors and provide the spectral isolation needed to provide radiances in

734 well-defined spectral intervals. Accurate specification and characterization of the filters is essential

735 as they and the detectors provide the overall instrument spectral response. The spectral response

736 functions are used in the process of deriving all SABER data products. Component level testing

737 and analysis of the SABER spectral response is described by *Hansen et al.*, (2003).

738 **Table 17**. SABER optical filter parameter values.

Channel Number	Cut-On			Cut-Off			Avg. Transmission Between HPP	Avg. Out-of-Band Transmission	Long Wavelength Blocking Limit
	5% Absolute		Slope	5% Absolute		Slope			
	(cm^{-1})	(μm)	(%)	(cm^{-1})	(μm)	(%)	(%)	(%)	(μm)
1	698.2	14.323	1.27	648.2	15.427	1.13	74.4	≤0.05	22.4
2	760.2	13.154	1.61	577.45	17.319	1.77	90.7	≤0.03	24.4
3	606.2	13.154	1.61	577.45	17.319	1.77	90.7	≤0.03	24.4
4	1144.8	8.735	1.38	1012.9	9.873	1.03	88.1	≤0.02	15.5
5	1565.0	6.390	1.4	1369.1	7.304	1.00	86.5	≤0.02	12.5
6	1941.1	5.152	0.92	1864.4	5.364	1.47	70.9	≤0.01	10.0
7	2387.9	4.188	0.28	2303.4	4.341	0.51	70.6	≤0.01	10.0
8	5153.4	1.940	1.04	4511.0	2.217	0.88	85.9	≤0.01	10.0
9	6420.5	1.558	0.99	5750.2	1.739	0.98	83.7	≤0.01	10.0
10	7965.2	1.255	1.06	7710.6	1.297	0.69	60.7	≤0.01	5.0

739

740   Figure 19 shows the detector ceramic circuit board populated with detectors, JFETs,

741 feedback resistors, and feedback capacitors. The height of each detector was adjusted to correct

742 for the chromatic aberration caused by the filters. Electrical connections to the detector assembly

743 were made by soldering shielded stainless steel wires to the radially protruding pins. Shielded

744 stainless steel wires were used to minimize thermal conduction from the warm electronics to the

745 detector assembly.

746

747 **Figure 19.** Populated detector ceramic circuit board installed in the bottom part of the detector

748 assembly.

749   Figure 20 shows the filter assembly installed in the bottom part of the detector assembly as

750 well as showing the top part of the detector assembly welded to the bottom part of the detector

751 assembly. This figure also shows the FPA purge tube protruding from the side wall of the top part

752 of the detector assembly, and the pin on the top of the detector assembly that was used to clock the

753 Lyot stop. This ensured the Lyot stop struts were aligned with the image of the secondary mirror

754 support struts.

755
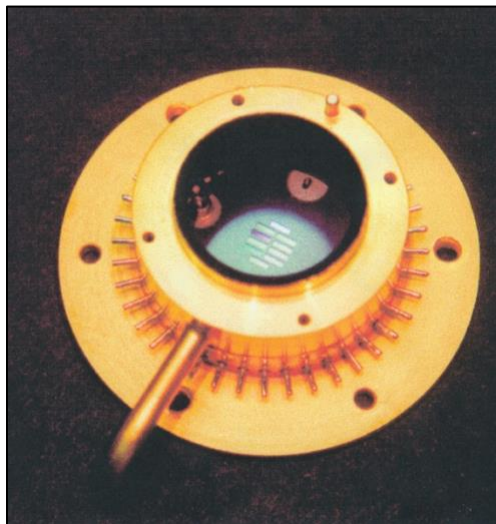
756 **Figure 20.** Filter array installed in bottom part of detector assembly and top part of detector

757 assembly welded to the bottom part of the detector assembly.

758 *4.8 SABER Fiber Support Technology (FiST)*

759   The SABER FPA assembly mount, which is shown in Figure 21, uses what SDL refers to

760 as Fiber Support Technology (FiST). This was a novel technique when SABER was built and

761 allowed the achievement of low thermal conduction from the telescope to the detector and the

762 cryocooler thermal link by using Kevlar fiber. This mount is very stiff with a first natural frequency

763 well above 500 Hz. The SABER FiST is bolted to the telescope at the three lapped pads on the

764 outer mounting ring (aluminum colored) in Figure 21. Pretensioned Kevlar strings support the

765 inner pedestal where the FPA is bolted. A very thin sheet, approximately 0.002" thick, was

766 sandwiched between the FPA and the FiST pedestal to maximize the thermal conductance between

767 them. A very flexible solderless thermal link with static stiffness measured to be less than 0.1

768 N/mm in all axes and a high thermal conductance (2.3 K/W) was bolted to the bottom surface of

769 the FiST pedestal and to the cryocooler cold block.

770
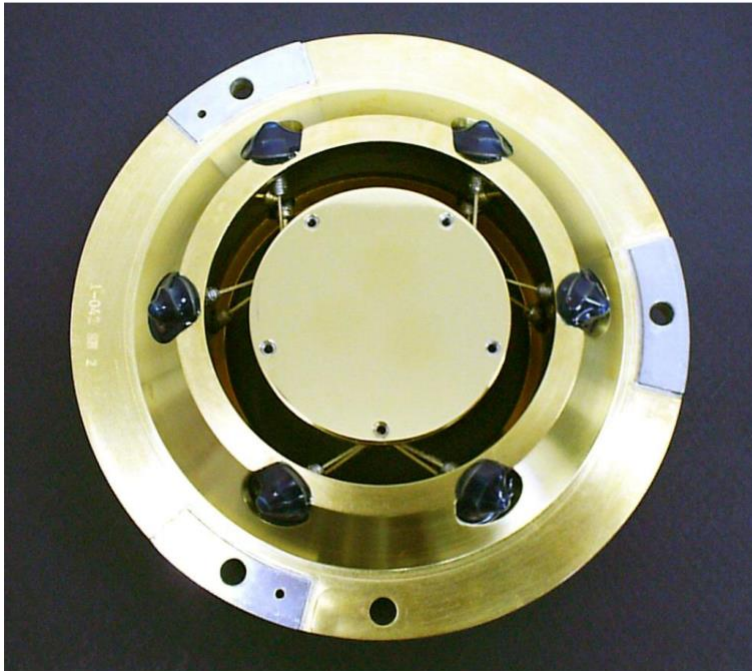
771 **Figure 21.** SABER Fiber Support Technology

772

4.9 SABER Lyot Stop

774   The SABER Lyot Stop is shown mounted on the top of the FPA in Figure 22 and is shown

775 as item N in Figure 2. It is a novel 3-dimensional design that blocks light scattered and diffracted

776 from the edges of the aperture stop, the secondary mirror baffle, and the secondary mirror support

777 struts. Diffracted and scattered light from the edges of the aperture stop, which is few mm in front

778 of the primary mirror, is blocked by the outside edge of the circular Lyot stop opening that can be

779 seen in Figure 22. Diffracted and scattered light from the edges of the secondary mirror baffle is

780 blocked by the inner edge of the central obscuration of the Lyot stop. Diffracted and scattered light

781 from the three secondary mirror struts is blocked by the Lyot stop struts. The SABER Lyot stop

782 protrudes through the central hole of the tertiary mirror as can be seen in Figure 23.
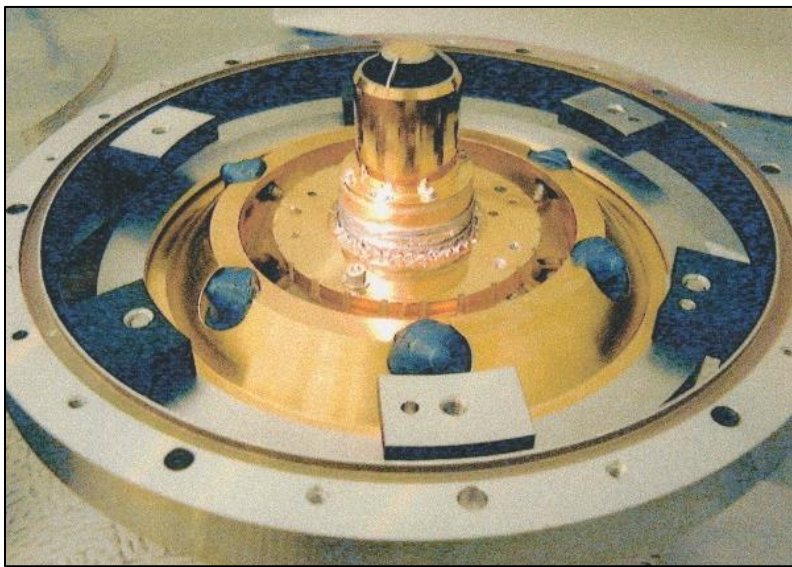
Figure 22. Lyot stop mounted to the top of the FPA

786
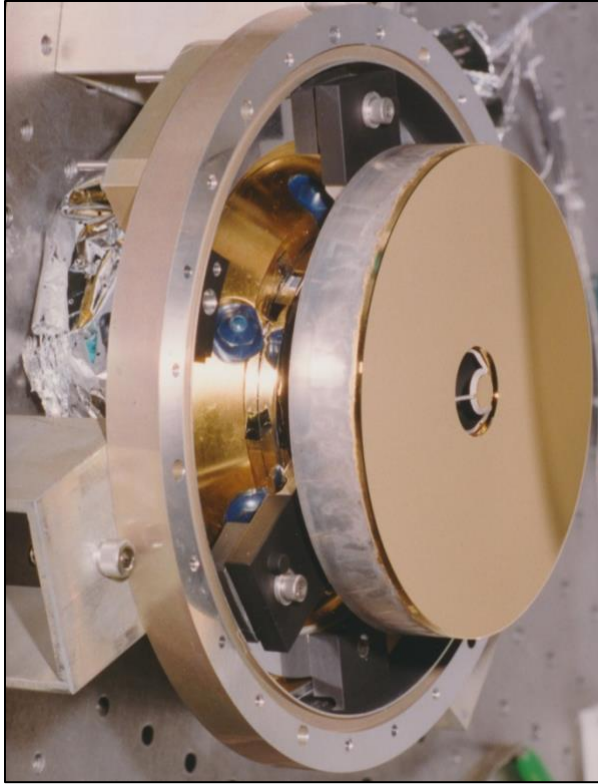
Figure 23. The SABER Lyot stop protrudes through a hole in the center of the tertiary mirror

788

4.10 SABER Cryocooler

Figure 24 shows the pulse-tube cryocooler used in SABER and developed by the TRW Corporation in the mid-1990s. At the time SABER was built, this cryocooler was known as a miniature cryocooler. This cooler has now been operating nearly continuously in space for over 21 years. The only time it has been turned off has been to enable evaporation of cryo-films that are deposited over time on the FPA, flex link and cooler cold tip due to outgassing of MLI on the outside of the SABER instrument, the other TIMED instruments, and the TIMED spacecraft. Before launch, this cryocooler was run for several months in a US Air Force testing laboratory. The approach to cooling SABER with this device is given in *Jensen et al*. (1998).

50

798
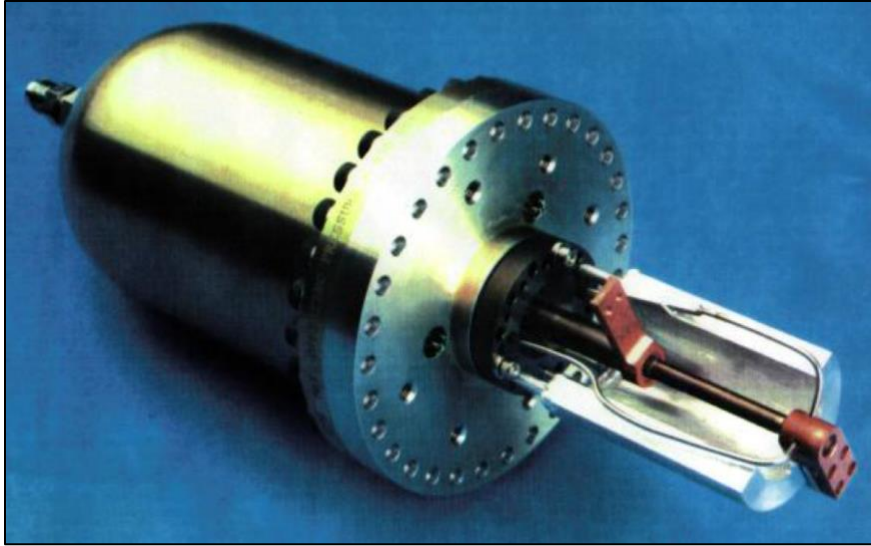
Figure 24. TRW miniature pulse tube cryocooler used for SABER.

800

4.11 SABER Electronics

There are two types of analog signal processing channels in SABER, one type for PC detectors and the other for PV detectors. The only configuration difference between these two types is the preamplifiers. Preamplifiers for PC detectors use a voltage amplifier in the operating temperature range of 245 K to 262 K to amplify the voltage across a biased PC detector operating at 75 K. The preamplifiers for PV detectors use a TIA to amplify the current from the PV detectors. The PV detector, a matched JFET pair, a feedback resistor, and a feedback capacitor are all operating at 75 K while the operation amplifier that closes the feedback loop is operating in the range of 245 K to 262 K. Thermal isolation between these two temperature zones is achieved by using shielded stainless steel wires.

The remaining analog signal path architecture is the same for both PC and PV channels. The preamplifier is followed by an instrumentation amplifier, which is followed by a 3-pole Bessel bandpass filter centered on 1000 Hz, which is followed by a coherent rectifier stage that is phase locked with the chopper, which is followed by a 4-pole low-pass Butterworth filter with a 4.545

815   Hz NEBW, which is followed by an voltage off-set adjustment stage, which is followed by a gain

816   ranging stage with three gains, which is followed by a voltage follower stage to provide output

817   isolation into a multiplexer, which is followed by a single instrument amplifier, which feeds a

818   single sample-and-hold amplifier, which feeds a single 12-bit ADC, which feeds a 1553 interface

819   stage, which finally feeds the TIMED Spacecraft electrical interface. The electronic power

820   breakdown at the board level and by operation mode is given in Table 18.

821

822   **Table 18**. Electronic power breakdown at the board level and by operational mode.

Board Names	System	Calibration, Data Collection, Diagnostic Modes		Standby, Stabilization Modes		Power-up, Safe Modes	
		Avg. (watt)	Peak (watt)	Avg. (watt)	Peak (watt)	Avg. (watt)	Peak (watt)
PC Channels 1-5	Signal Processing	2.3	2.3	2.3	2.3	0.0	0.0
PV Channels (6-10	Signal Processing	2.2	2.2	2.2	2.2	0.0	0.0
Mux-A/D Converter	Signal Processing	1.0	1.0	1.0	1.0	0.0	0.0
DC/DC Converters (3)	Power	3.4	3.4	3.4	3.4	0.0	0.0
DC/DC Converters (4)	Power	8.3	10.4	8.3	8.3	0.0	0.0
DC/DC Converters (1 and 2)	Power	6.6	15.3	6.6	6.6	2.5	2.5
BB/JS/Heaters/Chop Cont & Sync	Analog Controllers/Chopper	0.9	3.3	0.9	0.9	0.0	0.0
Sys. Cntrl/Formatter/1553	Sys. Control & Data Handling	1.3	1.3	1.3	1.3	1.3	1.3
Scan Mirror Control/Driver	Scan Mirror Controller	1.2	1.5	1.2	1.2	0.0	0.0
Housekeeping (2)	Sys. Control & Data Handling	1.2	1.2	1.2	1.2	1.2	1.2
Housekeeping (1)	Sys. Control & Data Handling	0.6	0.6	0.6	0.6	0.6	0.6
Totals		29.0	42.5	29.0	29.0	5.6	5.6

823

824   **Summary**

825   The SABER instrument has been in orbit since 7 December 2001 and making routine

826   science operations since 22 January 2002. As of this writing the instrument continues nominal

827   operations. All standard data products are being produced on a regular schedule and made available

828   to the public. More than 2,200 peer-reviewed journal articles have been published by scientists

829   worldwide. The instrument has proven to be remarkably stable in its calibration after more than 21

830   years in orbit despite having an original planned mission life of 2 years. This remarkable and

831   sustained scientific output from SABER is attributable to the excellent quality of the radiances

832   measured by the SABER instrument and the excellent characterization of the instrument during its

833   development and testing. In this paper we have described the major systems and subsystems that

834   comprise the SABER instrument. It is evident that the skill and care taken to design, build,

835   calibrate, and operate SABER are major factors in its long lifetime and subsequent scientific

836   productivity.

837

838   **Open Research**

839   This paper provides a detailed technical description of the SABER instrument. There are

840   no scientific results reported herein and consequently no datasets to report. More detailed

841   information related to the procedures and tests used to calibrate the SABER instrument are

842   included in the SABER Ground Calibration report provided to NASA Langley by SDL. This report

843   and a separate file listing reference citations to the 2200 peer-reviewed journal articles using

844   SABER data are included as Supporting Information.

845

Reference Citations

Brown, S. M. Jensen, S. Jensen, G. Hansen, L. Zollinger, R. Esplin, J. B. Miller, (2006). Sounding
of the atmosphere using broadband emission radiometry (SABER): sensor design,
performance, and lessons learned, Proceedings of SPIE 6297, doi: 10.1117/12.684137

Dyer, J., S. Brown, R. Esplin, G. Hansen, S. Jensen, J. Stauder, and L. Zollinger, (2002).
Contamination Control of the SABER Cryogenic Infrared Telescope. Proceedings of
SPIE 4774, https://doi.org/10.1117/12.481652

Hansen, S., J. Peterson, R. Esplin, and J. Tansock, (2003). Component level prediction versus
system level measurement of SABER relative spectral response, International Journal of
Remote Sensing, https://doi.org/10.1080/01431160304968

Jensen, S., J. C. Batty, W. A. Roettker, M. J. Felt, (1998). Cooling SABER with a miniature pulse
tube refrigerator, Proceeding of SPIE 3435, https://doi.org/10.1117/12.323740

Mlynczak, M. G., L. A. Hunt, R. R. Garcia, V. L. Harvey, B. T. Marshall, J. Yue, C. J. Mertens,
and J. M. Russell, (2022). Cooling and contraction of the Mesosphere and Lower
Thermosphere from 2022 to 2021, *J. Geophys. Res. – Atmospheres*,
https://doi.org/10.1029/2022JD036767

Mlynczak, M. G., J. Yue, J. McCormack, R. S. Liebermann, and N. J. Livesey (2021), An
observational gap at the edge of space, *Eos, 102,* https://doi.org/10.1029/2021EO155494.

Mlynczak, M. G., et al., (2020). Radiometric stability of the SABER instrument. Earth and Space
Science, https://doi.org/10.1029/2019EA001011

Mlynczak, M. G., (1997) Energetics of the mesosphere and lower thermosphere and the SABER
experiment, *Advances in Space Research*, Volume 20, Issue 6, 1997, Pages 1177-1183,
https://doi.org/10.1016/S0273-1177(97)00769-2

888   Mlynczak, M. G., (1996). Energetics of the middle atmosphere: Theory and observation

889   requirements, *Advances in Space Research,* Volume 17, Issue 11, Pages 117-126,

890   https://doi.org/10.1016/0273-1177(95)00739-2.

891   Mlynczak, M. G., S. Solomon, (1993). A detailed evaluation of the heating efficiency in the

892   middle atmosphere, *J. Geophys. Res*., 98(D6), 10517-10541, 10.1029/93JD00315.

893   Russell III, James M., M. G. Mlynczak, L. L. Gordley, J. J. Tansock, Jr., and R. W. Esplin,

894   (1999). Overview of the SABER experiment and preliminary calibration results Proc.

895   SPIE 3756, 277 (1999), DOI:10.1117/12.366382.

896   Stauder, J., R. Esplin, L. Zollinger, M. Mlynczak, J. Russell III, L. L. Gordley, and B. T.

897   Marshall, Stray light analysis of the SABER telescope, Proceedings of SPIE 2553,

898   https://doi.org/10.1117/12.221362

899   Tansock, J., et al. (2003). SABER ground calibration. International Journal of Remote Sensing,

900   24(2), 403–420. https://doi.org/10.1080/01431160304969

901